



3 Non-Invasive and Non-Destructive Examination 4 of Artistic Pigments, Paints, and Paintings by Means 5 of X-Ray Methods

6 Koen Janssens¹  · Geert Van der Snickt^{1,2} ·
7 Frederik Vanmeert¹ · Stijn Legrand¹ ·
8 Gert Nuyts¹ · Matthias Alfeld^{1,3} · Letizia Monico^{1,4} ·
9 Willemien Anaf^{1,5,7} · Wout De Nolf^{1,6} ·
10 Marc Vermeulen^{1,7} · Jo Verbeeck⁸ · Karolien De Wael¹

11
12 Received: 15 May 2016 / Accepted: 21 October 2016
13 © Springer International Publishing Switzerland 2016

14 **Abstract** Recent studies are concisely reviewed, in which X-ray beams of (sub)mi-
15 crometre to millimetre dimensions have been used for non-destructive analysis and
16 characterization of pigments, minute paint samples, and/or entire paintings from the
17 seventeenth to the early twentieth century painters. The overview presented encom-
18 passes the use of laboratory and synchrotron radiation-based instrumentation and
19 deals with the use of several variants of X-ray fluorescence (XRF) as a method of
20 elemental analysis and imaging, as well as with the combined use of X-ray diffraction
21 (XRD) and X-ray absorption spectroscopy (XAS). Microscopic XRF is a variant of the
22 method that is well suited to visualize the elemental distribution of key elements,
23 mostly metals, present in paint multi-layers, on the length scale from 1 to 100 µm
24 inside micro-samples taken from paintings. In the context of the characterization of
25 artists' pigments subjected to natural degradation, the use of methods limited to ele-
26 mental analysis or imaging usually is not sufficient to elucidate the chemical

A1 This article is part of the Topical Collection “Analytical Chemistry for Cultural Heritage”.

A2  Koen Janssens
A3 koen.janssens@uantwerpen.be

A4 ¹ AXES Research Group, Department of Chemistry, University of Antwerp, Antwerp, Belgium

A5 ² Conservation/Restauration Department, University of Antwerp, Antwerp, Belgium

A6 ³ Laboratoire d'Archéologie Moléculaire et Structurale, Pierre and Marie Curie, Paris, France

A7 ⁴ Department of Chemistry, Biology and Biotechnologies, Centro SMAART and CNR-ISTM,
A8 University of Perugia, Perugia, Italy

A9 ⁵ Royal Museum of Fine Arts, Brussels, Brussels, Belgium

A10 ⁶ Experimental Division, European Synchrotron Radiation Facility, Grenoble, France

A11 ⁷ Royal Institute for Cultural Heritage, Brussels, Belgium

A12 ⁸ EMAT Research Group, Department of Physics, University of Antwerp, Antwerp, Belgium



transformations that have taken place. However, at synchrotron facilities, combinations of μ -XRF with related methods such as μ -XAS and μ -XRD have proven themselves to be very suitable for such studies. Their use is often combined with microscopic Fourier transform infra-red spectroscopy and/or Raman microscopy since these methods deliver complementary information of high molecular specificity at more or less the same length scale as the X-ray microprobe techniques. Since microscopic investigation of a relatively limited number of minute paint samples, taken from a given work of art, may not yield representative information about the entire artefact, several methods for macroscopic, non-invasive imaging have recently been developed. Those based on XRF scanning and full-field hyperspectral imaging appear very promising; some recent published results are discussed.

Keywords X-ray fluorescence · X-ray diffraction · X-ray absorption · Synchrotron radiation · Paintings · Pigments

1 Introduction

Starting from pre-historic times, human artists have always felt the urge to depict their surrounding world on various substrates by using colored materials of different types. Historical paintings, such as, for example, prehistoric cave paintings, are often called “windows on the past” and have allowed later generations to imagine how former human societies looked and/or functioned. Historical paintings, therefore, are an enormously valuable part of the cultural legacy we have inherited from past generations.

There is a general belief that paintings are complex, but essentially static assemblages of widely different (in)organic materials. However, at, or just below, the seemingly placid surface of these works of art, chemical reactions are taking place that slowly alter the chemical make-up of the paint layers. While some of these reactions are the result of intimate contact between the different materials, most are driven forward by external physicochemical factors. A prime stimulus for reduction–oxidation (redox) reactions is light absorption by colored substances (molecules) in the ultraviolet (UV) and visible (VIS) range. Such reactions can lead to spontaneous in situ formation of secondary chemicals that will often differ in their macroscopic properties (such as color, volume, porosity) from the original materials. Both the organic components of paint (protein-, saccharide- or lipid/oil-based binding media, organic dyes, etc.) and/or the inorganic components (mostly pigments based on metal ions) may be affected. Another important factor in paint degradation is the often cyclic variation in relative humidity, which causes condensation and re-evaporation of minute moisture droplets within the microporous, age-cracked paint layers. The latter can act as miniature galvanic cells in which redox reactions can occur at the interface between pigment grains, binding medium, and water. In addition, phenomena such as crystallization of salts, the leaching of metal cations from pigment grains, and in situ formation of metal soaps can gradually undermine the mechanical integrity of paint materials [1]. Cycles of condensation/evaporation may also transport secondary alteration compounds



towards the surface, leading to the formation of weathering crusts. These crusts can be partly crystalline; almost all have a color and texture that is quite different from the original material.

When considering the inorganic materials employed as pigments by artists from the fifteenth to the eighteenth century, a relatively limited evolution can be observed over time. This is because the chemistry of pigment synthesis was fairly limited in this period, with the majority of inorganic materials used as pigments still being naturally occurring minerals. Only in cases of a few exceptions, such as lead white and smalt, the chemical technology was sufficiently advanced that specific colored inorganic materials of high quality and chemical stability could be synthesized in controlled circumstances.

Since the trade in artists' pigments was well spread, it was possible for artists to purchase different varieties of the same pigment, often of significantly different quality and price; in the case of mineral species, these quality differences are related to different geographical origins and/or the grain selection/purification method to convert mineral finds into finely ground pigment powder.

Among the pigments employed by fifteenth to seventeenth century fine art painters in the Low Countries, such as Jan Van Eyck (1390–1441), Hans Memling (1430?–1494), Quinten Matsys (1466–1530), Pieter Brueghel the Elder (1525?–1569), Pieter Paul Rubens (1577–1640), Anthony Van Dyck (1599–1641), Rembrandt van Rijn (1606–1669), Jan Davidz. de Heem (1606–1684), and Johannes Vermeer (1632–1675), a few fall in a special category. For these, in many historical paintings, a significant level of chemical alteration of either the pigment grains themselves or of the paint they are part of is observed. It concerns, for example, the pigment smalt (a blue, cobalt-doped type of potassium-rich glass), vermilion red (mercury sulphide, HgS , also known as cinnabar in its mineral form, a pigment used since antiquity), orpiment and realgar (both arsenic sulphides, respectively As_2S_3 and As_4S_4), and lead white (usually a mixture of cerussite, PbCO_3 , and hydrocerussite, $2\text{PbCO}_3 \cdot \text{Pb}(\text{OH})_2$). Smalt is a very frequently employed blue pigment that turns greyish/pink upon alteration. Since smalt is often used as part of large surfaces (for example, in a blue sky, in blue clothing of saintly figures, in the darker backgrounds of indoor scenes) its discoloration can have a profound influence of the general outlook and color balance of the painting. This is, for example, the case in a number of paintings by Jan Matsys (1509–1573) and Rembrandt van Rijn. A less strong, but notable change in color can take place with vermilion red, where the originally bright red surface may darken; in addition, the blackened parts of the paint often become covered with white precipitates. In a number of works by the baroque-era painters P.P. Rubens and Pieter Brueghel the Younger (1564–1636), such discolorations have been observed. The yellow/orange pigments composed of arsenic sulphides such as realgar and orpiment have a reputation of being fugitive, i.e., one assumes them to be converted by the action of light and humidity to gaseous/volatile As-containing compounds, supposedly causing the yellow-orange tinting power of these paints to slowly disappear. The seventeenth century painter J. Davidz. de Heem frequently employs the bright orange orpiment as part of his intricate flower pieces while in the Rembrandt



paintings *The Nightwatch* and *The Jewish Bride*, realgar is for example employed for painting yellow/golden highlights of the fabrics.

Near the end of the nineteenth century, a number of scientific and technical innovations such as the industrial synthesis of new pigments (with bright, more saturated hues) and the introduction of the paint tube (allowing easy distribution and use of industrially produced artistic paints) set the stage for a significant artistic revolution. Indeed, several masters of modern art, such as Joseph M.W. Turner (1775–1851), John Constable (1776–1837), Camille Pissarro (1830–1903), Paul Cézanne (1839–1906), Vincent van Gogh (1853–1890), George Seurat (1859–1891), and James Ensor (1860–1949) avidly made use of the new possibilities the recently available pigments and paints offered for expressing themselves.

Among the many colors employed by Vincent Van Gogh, the use of yellow pigments becomes very important after 1885. While in his early period (1883–1885/6), he employed mainly Naples yellow (lead antimonate) or light hued earth pigments, in the second half of his career (when he worked in Paris, Arles, and St. Remy, 1885–1890), he frequently employs both chrome yellow and cadmium yellow [2]. As becomes clear from his correspondence [3], chrome yellows are among Van Gogh's favored pigments, featuring in some of his most important paintings from the French period (1886–1890), such as, for example, the *Sunflowers* series of paintings. Already during his lifetime, Vincent van Gogh was aware of the lack of stability of chrome yellow (see letter nr. 595 from 1898 [3]). In this respect, cadmium yellow had a better reputation; however, recent investigations have revealed that also this pigment may change its hue under the influence of time and environmental agents. Its degradation behavior has been/is being studied in works of art by Vincent Van Gogh, Henri Matisse (1869–1954), and Edvard Munch (1863–1944). The final pigment to be discussed here is minium or red lead (Pb_3O_4); Van Gogh and his contemporaries sometimes employed this orange-red pigment. This substance, frequently used outside artists' workshops to protect metals from corrosion, tends to become either white or black, as a function of its chemical environment.

In order to assess better the current and future state of a painted work of art, it is highly relevant to have a good understanding of the alteration processes that gradually affect the materials it consists of. Many of these alteration phenomena only become visible after an extended period of time and are caused by slow acting (physico-)chemical transformations in multi-component and multi-phase chemical systems that only gradually move towards equilibrium. Redox processes have been identified as being responsible for alteration of a number of inorganic pigments. A lot of these reactions involved include a photo-activation step and, therefore, require (sufficiently energetic) light falling on the painting (surface). The secondary compounds formed in this manner generally are present as micrometer-thin layers, at or just below the paint surface. Advanced analytical methods that allow to distinguish between subtly different compounds or valence states of the same transition metal in these micrometer-thin and superficial alteration layers and that at the same time are able to provide information on the distribution of such secondary compounds, are therefore mandatory tools for art-conservation research [4].

Traditionally, to study the chemical make-up of painted artworks in detail, (minute) paint samples are collected. These tiny samples can be taken using five



standard “microdestructive” techniques: scalpels or lancets (e.g. [5]); gentle cotton bud (Q-tip) abrasion (e.g. [6]); microdrilling (involving a 100–200 μm diameter bore) (e.g. [7]); or laser ablation, the ablated materials being collected on microscope slides (e.g. [8]). These techniques remove only minute amounts of material and any damage is effectively invisible to the naked eye; they, therefore, do not disturb the esthetic experience of the artwork. Moreover, microdestructive sampling is mostly limited to areas where paint losses have already occurred. The extracted material often comprises the entire stack of micrometre-thick paint layers at a given position. To examine the minute samples, one or more non-destructive microanalytical methods may be employed before undertaking additional analytical investigations that involve the chemical digestion of the sampled material, or any other wet-chemical operation. Prior to microanalysis, multilayered paint samples are typically embedded in resin, cross-sectioned and then polished. Alternatively, the different materials/layers in a paint sample may be carefully separated from each other under the microscope for separate analysis.

The range of analytical techniques available to painting researchers is now fairly extensive and the methods can be used to characterize a painting’s materials in detail. They include the following: optical microscopy (OM), scanning electron microscopy coupled with energy dispersive X-ray spectrometry (SEM-EDX) [9], micro-Fourier transform infrared spectroscopy (μ -FTIR) ([10]), micro-Raman spectroscopy (μ -RS) [11, 12], high-pressure liquid chromatography (HPLC), gas chromatography coupled with mass spectrometry (GCMS), and pyrolysis GCMS (Py-GCMS) [5, 13–15]. To complement these analytical methods there are chemical imaging techniques such as synchrotron radiation (SR)-based micro-X-ray fluorescence (μ -XRF) [16], micro-X-ray absorption near-edge spectroscopy (μ -XANES) spectroscopy ([17]), micro-X-ray powder diffraction (μ -XRPD) [18], and synchrotron radiation micro-Fourier transform infrared spectroscopy (SR- μ -FTIR). SR-based photoluminescence is a relative new addition to this series [19]. Often, combinations of these methods are required to fully understand the paints’ chemistry [20, 21]. This was also the case for a number of the investigations described below.

Micrometers below a painting’s surface, a wealth of information may be present about the creative process followed by the artist while making the work of art. The manner in which a painted work of art was created, its conservation, and exhibition history may leave material traces behind, for example, in the layer-by-layer build-up of the artwork. However, this stratigraphic information, comprising structural and compositional aspects, is usually not easy to obtain in a non-invasive manner. Next to the visible surface layers, subsurface layers may include underdrawings, underpaintings, and adjustments made in the course of painting. Together, all these layers determine the current appearance of the work of art. In a growing number of cases conservators have discovered abandoned compositions underneath paintings, illustrating the artist’s practice of reusing a canvas or panel. Imaging methods that can “read” this hidden information without any damage to the artwork are, therefore, valuable tools for art-historical research [22]. The standard methods for studying the inner structure of painted works of art are X-ray radiography (XRR) and infrared reflectography (IRR), both penetrative illumination techniques that are optionally complemented with the microscopic analysis of cross-sectioned paint samples. Since



these methods all have their limitations, recently, a number of fundamentally new approaches based on X-rays for imaging the buildup of hidden paint layers systems (and for analyzing small samples thereof) have been put into practice. Two major motivations can be discerned for the development of such analytical methods: (a) the desire to know more about the creative process and/or the artist's way of working that have led to a given artefact and (b) the need to assess and predict the current and future condition of a work of art. Motivation (a) is essentially of art-historical nature and seeks to reconstruct (better) the *past/history* of an artwork while motivation (b) is more strongly linked to preventive conservation and to conservation technology and, therefore, mostly concerned with *the future* of the artwork [17]. It should be duly noted, however, that for conservation, also an understanding of the history of a work of art and the artist's intent is fundamental, since it provides the basis for assessing the current condition of the artwork and for deciding which might be the most appropriate interventions [23].

A comprehensive understanding of the paints used in a work of art, therefore, requires information from across the painting's surface, as well as on their ordering as a function of depth [23]. To complement the detailed information that can be gathered from a limited number of (possibly non-representative) paint cross sections, mobile versions of different non-invasive spectroscopic methods can be used to investigate a (much) larger number of locations on a work of art. By means of portable XRF (PXRF), element signatures can be swiftly recorded from all differently colored areas of a painting, allowing indirect inferences to be made on which pigments were used throughout. Similarly, portable RS and FTIR equipment can be used in a complementary manner to record molecular spectroscopic data and to assess the presence of any organic constituents (e.g. [24]). More recently, several X-ray and visible/near infrared (VIS/NIR) based non-invasive imaging methods have been developed and successfully employed to document the composition of *complete* paintings [25–27]. They can be considered the state-of-the-art equivalents of the two imaging methods that have been routinely employed in subsurface investigation of paintings for several decades: infrared reflectography (IRR) and X-ray radiography (XRR). Some of these exploit a scanning mode of operation (see Fig. 1) and include the techniques of macroscopic X-ray fluorescence (MA-XRF) [26], macroscopic X-ray diffraction (MA-XRD) [28], macroscopic Fourier transform infrared scanning in reflection mode (MA-rFTIR) [29], and VVIS/NIR imaging [30]. Camera-based analytical approaches include hyperspectral imaging in the visible range (350–700 nm), the near-infrared range (NIR; 0.7–1.7 μm), and the short-wave infrared range (SWIR; 1.7–2.5 μm) [27].

In what follows, after outlining a number of X-ray based methods of analysis suitable for studying pigment degradation phenomena, we describe a number of recent studies aimed at unraveling the degradation pathways these pigments are subjected to. Here, the ability to determine the speciation of the inorganic metallic compounds on the (sub)microscopic scale is often highly valuable, as this speciation state often alters during degradation processes. We also briefly describe recently developed methods of chemical imaging by means of which the distribution of pigments in paintings can be visualized. It is often interesting to combine both methods for local (speciation) analysis and large scale chemical imaging in a study of a particular work of art.



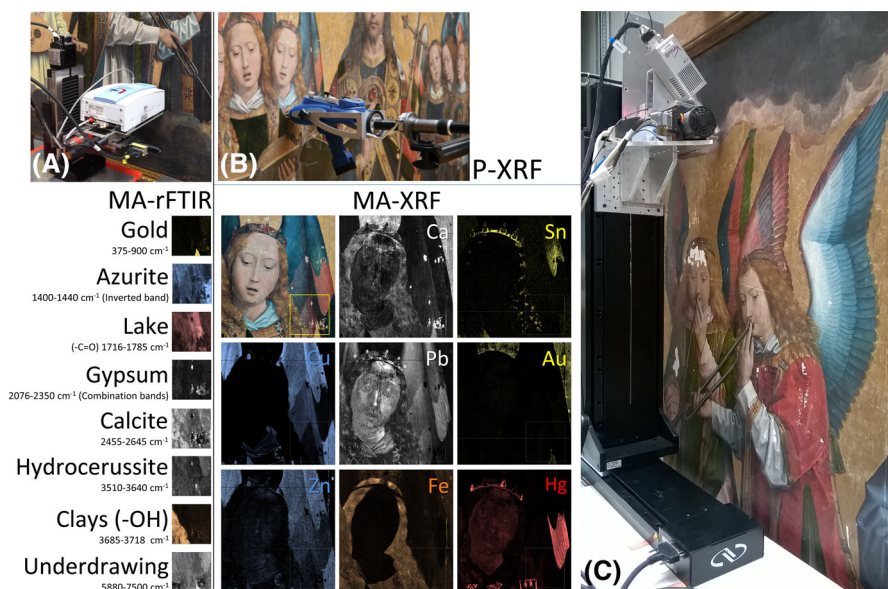


Fig. 1 *Christ with singing and music-making Angels*, Hans Memling (1430–1495, Royal Museum of Fine Arts, Antwerp, Belgium, panels 779, 778, and 780; oil on panel). **a** MA-rFTIR scanner in front of panel 779; **b** PXRF-analysis of the chest-area of Angel #8, panel 778. **c** MA-XRF scanner, scanning part of panel 780, and resulting elemental maps. The FTIR maps shown in **a** correspond to the white rectangle in the MA-XRF maps shown in **c**. Adapted from [21]

256 2 X-ray Based Methods of Analysis

257 X-ray fluorescence analysis (XRF) is a well-established method of (semi-)
 258 quantitative elemental analysis that is based on the ionization of the atoms of the
 259 material being irradiated by an energetic beam of primary X-rays. XRF on heritage
 260 and archaeological samples is mainly used in reflection geometry to probe the
 261 stratigraphy of polished cross-sections of micro-samples or the exposed surfaces of
 262 objects. The energy of the fluorescent photons is the difference in energy between
 263 the vacancy that is the result of the ionization process and the electronic state of the
 264 electron filling the vacancy [16, 31]. In this manner, the characteristic radiation
 265 emitted by the ionized atoms contains information on the nature and the abundance
 266 of the elemental constituents present. The technique is particularly efficient for
 267 studying high atomic number (high-Z) elements in low-Z matrices. Analysis of the
 268 XRF spectra involves identification of the elements present from the fluorescence
 269 lines observed and estimation of their net intensity; the latter are in principle
 270 proportional to the abundance of the corresponding chemical elements. (Semi-)
 271 quantitative analysis usually involves more complex calculations as initial
 272 absorption of the X-ray beam and absorption of the fluorescent photons in the
 273 material has to be modeled by taking the (expected) matrix composition into
 274 account in an iterative fashion [32–34]. Since XRF meets a number of the
 275 requirements of the “ideal method” for non-destructive analysis of cultural heritage

materials [35], analysis of objects of artistic and/or archaeological value with conventional XRF is fairly common. It is in fact one of the most often applied methods for obtaining qualitative and semi-quantitative information on such objects. Several textbooks cover the fundamental and methodological aspects of the method and its many variants [36].

The variants of XRF that are most relevant for the analysis of painted works of art or of micro-samples taken from such artifacts are (1) PXRF, (2) the X-ray microprobe (XMP), involving the combined use of μ -XRF/ μ -X-ray absorption spectroscopy (μ -XAS) and/or of μ -XRF/ μ -XRD, usually based on synchrotron radiation, and (3) MA-XRF imaging.

Portable XRF (PXRF): prior to analyzing painted works of art with more sophisticated methods, as a means of first exploration or screening of the artifacts, the use PXRF, sometimes also called handheld XRF (HXRF or HHXRF) is usually very relevant [37]. Various compact, battery operated devices of this kind are now commercially available [38–43] next to a number of self-built systems [44–47]. One of these is shown in Fig. 1b. Since the interaction of individual photons of a specific energy with single atoms of given atomic number can be very well described, in principle, any form of X-ray fluorescence and, therefore, also PXRF, has the potential of being used for (semi-)quantitative analysis. Several calibration schemes and variants thereof have been developed since the 1970s [48]. Over the past decade, PXRF instruments have allowed non-invasive analyses to be conducted in museums around the world, on virtually any size artifact, producing data for up to several hundred samples per day. However, questions have been raised about the sensitivity, precision, and accuracy of these devices, and the limitations and advantages stemming from performing surface analysis on (often) heterogeneous objects made in obsidian, ceramics, metals, bone, and painted materials have been discussed [49]. In the next paragraph, a number of recently published studies in which PXRF was part of the set of analytical methods employed is outlined. Considering that in PXRF-based studies, the interpretation of the spectral data obtained from complex, multilayered (paint) systems can be problematic, usually the advantages of PXRF have been exploited in combination with other, more surface-specific and/or molecule-specific methods of analysis, in particular vibrational spectroscopies such as Raman and FTIR (micro)spectroscopy.

PXRF has been used extensively both for documentation, as well as for authentication purposes [50] of works of art of different historical periods. The painting materials used in prehistoric rock art have been characterized by PXRF, usually in combination with more specific methods (of molecular spectroscopy) [51–53]. To characterize the materials and stratigraphies of an Egyptian coffin in the Museo Civico Archeologico of Bologna (Italy), restored several times in the past, a two-step approach involving both non-invasive and micro-invasive analysis techniques was used [54]. The in situ, portable spectroscopies employed included XRF, fibre optics reflectance spectroscopy (FORS), and FTIR. This multi-technique approach allowed to reveal many differences in the composition of the (calcite, CaCO_3) ground layer and to identify the pigments in the original [cinnabar, orpiment, red clay, Egyptian blue ($\text{CaCuSi}_4\text{O}_{10}$), and copper-based greens] and restored zones [lead white, Naples yellow ($\text{Pb}(\text{SbO}_3)_2/\text{Pb}_3(\text{SbO}_4)_2$), cerulean blue



(CoO·nSnO₂), azurite (2CuCO₃·Cu(OH)₂) of the coffin. In order to resolve remaining doubts about the presence of specific pigments in superimposed layers, a few micro-fragments of paint were removed and analyzed using benchtop methods. PXRF was combined with portable RS, Diffuse reflectance infra-red Fourier transform spectroscopy (DRIFTS) and other methods for studying two wall paintings in the Naples Archaeological Museum. The artefacts were extracted ca. 150 years ago from Marcus Lucretius' house in Pompeii, showing the result of the interaction of H₂S gas (expelled during the eruption of Vesuvius) on the painting materials [55]. The efflorescence on the walls of the house and the extracted wall paintings were also studied [56]. The painted surface of plasters withdrawn from different areas of the Villa dei Quintili (Rome, Italy) were examined in a similar manner [57]. A combined XRF/XRD portable instrument was used to study the pigment palette in the paints of the vaults of the Courtyard of Lions in the Alhambra Palace (Granada, Spain), identifying (among others) cinnabar and hematite (Fe₂O₃) in the red hues, in combination with hydrocerussite in the flesh tones while lazurite ((Na,Ca)₈[(S,Cl,SO₄,OH)₂(Al₆Si₆O₂₄)]), azurite, and malachite (CuCO₃·Cu(OH)₂) were encountered in, respectively, the blue and green areas [58]. Nubian wall paintings (from churches in southern Egypt and northern Sudan) from the seventh to fourteenth century were analyzed with a combination of PXRF and LA-ICP-MS, allowing the identification of the raw materials employed [59]. On a thirteenth century icon covered by a nineteenth century painting, an extensive campaign of non-invasive analytical investigations was carried out using PXRF, FORS, UV–VIS absorption, and emission, allowing the documentation of the gilding techniques employed and formulation new hypotheses regarding thirteenth century painting techniques and materials [60]. To document the use of powdered bismuth (Bi) in Late Gothic paintings and polychromic sculptures, PXRF was used together with SEM-EDX and optical microscopy [61]. A combination of portable FTIR, Raman, and XRF was used to identify the rare minerals crocoite (PbCrO₄) and mimetite (Pb₅(AsO₄)₃Cl) in medieval Bohemian murals [62], probably as a result of the degradation of the pigments orpiment (As₂S₃) and minium (Pb₃O₄). The same methods were also employed to determine the nature of the painting materials present in Memling's polyptych *Angels Singing and Playing Music* [63] (see Fig. 1), allowing the assessment of the manner in which this painter employed a limited set of pigments and dyes to accomplish a great variety of color and optics effects. With the aim of establishing it better into its historical context, a portable XRF–XRD system was employed to analyze a fifteenth century illuminated parchment from the Archive of the Royal Chancellery in Granada [64]. This revealed the presence of gold and silver, lead tin oxide yellow (Pb(Sn,Si)O₃/Pb₂SnO₄), azurite, vermilion, minium, and malachite. Also, the materials employed by Pieter Brueghel the Elder in the painting *Mad Meg* were studied by means of PXRF and other methods [65], identifying the use of copper resinate green, smalt blue, vermilion red, and lead white; these findings confirm the hypotheses about “an economic way of painting” by Brueghel. The gold dust, gold leaf, and the materials used for the gilding of two miniature portraits on copper support from the Evora Museum collection (Portugal) were examined and analyzed by stereomicroscopy, Raman, and FTIR micro-spectroscopies, SEM-EDX, PXRF, and liquid chromatography coupled to diode



array and mass spectrometric detection [66]. The pigments and binding media employed in Sorolla's gouache sketches for the Library of the Hispanic Society of America, New York City, NY, USA have been studied by means of a combination of PXRF, SEM-EDX, and FTIR analysis, showing that a rich palette of pigments was used to manufacture these nineteenth century artists' materials [67]. With the aim of documenting the evolution in the pigment use of the late nineteenth century/early twentieth century. Belgian painter James Ensor, and to correlate this technical evolution with stylistic developments, a systematic survey was conducted mainly based on PXRF [68]. A series of non-invasive analyses employing PXRF, portable RS, and FTIR were combined with benchtop micro-Raman and SEM-EDX investigations to study the complicated mixtures encountered in paintings by E. Munch and F. Kupka, highlighting the need to employ combinations of methods in order to arrive at unambiguous pigment identifications [69]. Other works of modern painters were examined to verify their authenticity [70] or document their pigment usage [71–75].

Microscopic XRF (μ -XRF) is a branch of XRF that has been developed since 1990 [76], mainly thanks to the use and increasing availability of (a) synchrotron radiation (SR) and (b) various devices for efficient focusing of X-rays [16, 77]. It can obtain information on the local elemental composition of inhomogeneous samples. At synchrotron facilities, a variety of micro- or nanofocus optics, based on refraction [78, 79], diffraction [80, 81], or total reflection [82, 83] of X-rays, is currently in use to create small beams with energies in the 1–100 keV range and with diameters of typically 0.1–1 μ m. In laboratory μ -XRF instruments, mostly polycapillary lenses are employed for focusing [84–86], providing focused X-ray beams that usually are 10–30 μ m in diameter [87]. Among the commercial apparatus currently available, there are some specifically developed for the local investigation of works of art [88]. By incorporation of additional degrees of freedom of the measuring head, the analysis of Antique manuscripts [89, 90] and bronzes [91, 92], Medieval paintings [93], Chinese porcelain [94], and Baroque-era drawings [95] has become possible.

A specific sub-type of micro-XRF investigations are those employing a confocal excitation-detection geometry [96]. In this case, the recorded XRF signals stem from a well-defined cube-like “sampling” volume that is situated at the intersection of the X-ray optical devices positioned between X-ray source and sample (defining the primary beam) and between sample and X-ray detector (defining the direction from which XRF signals can enter the detector) [97]. Often, polycapillary optics are employed for the latter purpose [98, 99]. By moving the sample through this sampling volume, local information on the elemental composition of the material being investigated can be obtained. Sequential series of confocal XRF measurements along lines and planes allows to visualize the distribution of chemical elements of interest in one or two dimensions, creating, for example, virtual depth profiles, and two- or three-dimensional distributions inside the materials of interest [23, 100, 101]. After its original introduction at synchrotron radiation facilities [97, 101–105], the feasibility of performing confocal XRF measurements using tube sources was demonstrated by several groups around the world [106–110], along with appropriate deconvolution, quantification, and simulation models [111–118].



Several papers have been recently been published where confocal XRF measurements are exploited for sub-surface examination of painted works of art [119–124], next to pottery [125], coins [86], stained glass [126, 127], painted metal sheet [128], and natural rock samples [129].

About 10–15 years ago, the main advantages of SR-based μ -XRF for the study of archaeological and artistic materials (such as glass, inks, enamel, metals) were considered to be its quantitative and non-destructive character combined with the possibility to perform trace analysis at the 1–10 ppm-level for transition element metals [130]. At that time, the combined use of μ -XRF with μ -XAS and μ -XRD was described as an interesting development [131]. Currently, this multi-modal approach has become standard practice at SR facilities, where the role of μ -XRF is still central, but often no longer of major importance. X-ray microprobes (XMPs), i.e., synchrotron beam lines that allow the combined use of these methods are nowadays present at all SR facilities. Recent review papers [21, 132–134] indicate that they are well-established, non-destructive analytical tools that are successfully employed in a large variety of application fields such as materials science/quality control, environmental science, geology, and life sciences, as well as in cultural heritage investigations. Figures 2 and 3 show spectral data and chemical maps derived from degraded paint micro samples. For the investigation of (altered) paint layer samples, also SR-based μ -FTIR is being increasingly used as a complementary method; in addition to the identification of organic components (binders, varnishes) it provides

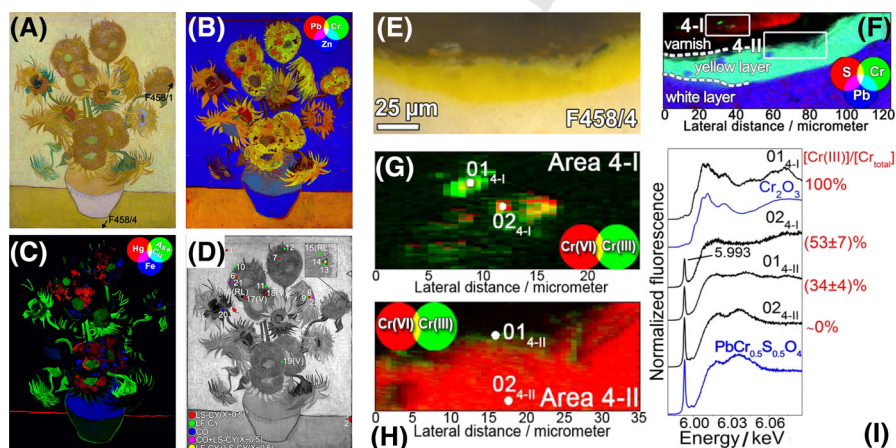


Fig. 2 a Photograph of *Sunflowers* by Van Gogh (Arles, 1889; Van Gogh Museum, Amsterdam, the Netherlands); sampling spots are also shown. RGB composite MA-XRF maps of **b** Pb/Cr/Zn and **c** Hg/As + Cu/Fe. **d** Raman and IR distribution of different CY types (LS-CY: light-sensitive chrome yellow ($\text{PbCr}_{1-x}\text{S}_x\text{O}_4$, with $x > 0.4$); LF-CY: light-fast chrome yellow (monoclinic PbCrO_4); CO: chrome orange ($[(1-x)\text{PbCrO}_4 \cdot x\text{PbO}]$). Triangles show the location of FTIR analyses; “V” and “RL” indicate spots containing also vermillion and red lead. The white circle denotes the location where only red lead was identified. **e** Photomicrograph detail of sample F458/4 where SR μ -XRF/ μ -XANES analysis of **f–i**) were performed. RGB SR μ -XRF images of **f** S/Cr/Pb [map size: $124 \times 51.2 \mu\text{m}^2$; pixel size ($h \times v$): $1 \times 0.25 \mu\text{m}^2$; energy: 6.090 keV]. **g**, **h** RG Cr(VI)/Cr(III) chemical state maps [pixel size ($h \times v$): $0.7 \times 0.2 \mu\text{m}^2$] and **i** XANES spectra collected from areas indicated in **g**, **b**. Maps of (**g**, **h**) were acquired in the regions shown in **f**. Adapted from [156]

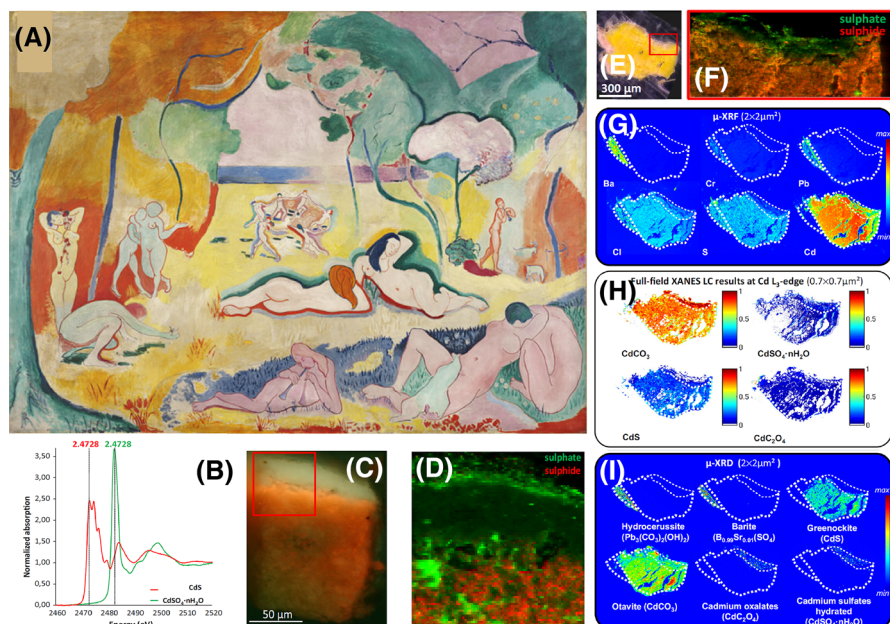


Fig. 3 **a** *Le bonheur de vivre* (aka *The Joy of Life*, 1905–1906, oil on canvas, 176.5 × 240.7 cm, The Barnes Foundation, BF719) by Henri Matisse; **b** S-Kα edge XANES of Cadmium yellow (CdS, in red) and its transparent/colourless oxidation product (CdSO₄·nH₂O, in green); **c**, **e** Optical photographs of paint cross sections taken from **a**; **d**, **f** Compound sulphide (red)/sulphate (green) map of the areas indicated by the red rectangle in respectively **c** and **e** (step size: 1 × 1.2 μm²); **g**–**i** XRF, full-field XANES and XRD maps of the sample shown in **e**. Adapted from [222]

specific information on the presence of counter ions such as carbonates, sulfates, and oxalates where μ-XRF and μ-XAS mostly yield data on the metal ions themselves.

SR-based XMPs have proven their value over more conventional combinations of microanalytical methods, especially for the characterization of degradation products that are formed in thin layers (smaller than 10 μm in thickness) at the surface of weathered archaeological and/or artistic materials and artifacts. Since individual paint layers in paint stratigraphies may be only a few micrometres in thickness, the lateral resolution offered by laboratory μ-XRF is not always sufficient to extract all relevant information; thus, the collection of elemental maps from paint cross sections using SEM-EDX at a typical lateral resolution of 1 μm is still preferred. Occasionally, μ-XRF has been used for this purpose, and then mostly in combination with other laboratory-based methods that provide complementary information [135, 136]. Since the use of (focussed beams of) synchrotron radiation exposes the materials under investigation to elevated doses of radiation, not all materials can be examined without beam damage [137]; phenomena such as gradual loss of crystallinity, beam-induced oxidation or reduction have been observed in several cases [138–140].

X-ray absorption spectroscopy (XAS) is based on the absorption of X-rays by materials in the vicinity of the absorption edge of one of its constituting elements.

The technique provides chemical speciation, i.e. information on the coordination sphere of the selected absorbing element (the central atom). The tunability of the synchrotron emission with typical bandwidths $\Delta E/E$ smaller than 10^{-3} – 10^{-4} , i.e. in the (fractional) eV range for hard X-rays, permits the fine scanning of individual element absorption edges. Synchrotron beam line setups are usually optimized to continuously scan the primary beam energy E with a fixed exit of the beam over the desired energy range (a few tens of electron volts for XANES or a few hundred eV for extended X-ray absorption fine structure (EXAFS) spectroscopy). Due to the high absorbance of many materials encountered at energies below 20 keV most X-ray absorption experiments for cultural heritage and archaeology are performed using XANES in fluorescence detection mode by collecting the X-ray signal typically over some tens of eVs. The XANES fingerprint that is obtained is compared to that of known reference compounds and in many situations the unknown fingerprint spectra can be described by a linear combination of the spectra of the references (see for example Fig. 2i or 3b). By recording μ -XRF maps at a limited number of energies along the XANES spectrum and appropriate transformation of the resulting intensity distributions, it is possible to obtain species-specific maps. Several reviews on the use of XANES for cultural heritage investigations are available [17, 20].

X-ray diffraction (XRD): the main use of XRD for the study of paintings and pigments stems from the fact that identification and quantification of crystalline phases in complex mixtures is possible. Via appropriate optics, an X-ray micro-beam of medium to low divergence (typically <3 mrad) is generated that allows a paint sample or an entire artifact either in transmission or in reflection geometry to be irradiated (see Fig. 4). Such beams may be generated at synchrotron facilities using various optics, but also by using laboratory X-ray sources and, e.g., double focusing mirrors. The powder diffraction rings are usually recorded with a two-dimensional detector and then azimuthally integrated (Fig. 4e, f), yielding a radial profile (scattering intensity vs. scattering angle 2θ or momentum transfer Q). Each phase inside the sample gives rise to a series of diffraction rings that appear as sharp peaks in the radial profile. This “fingerprint” can be compared with databases and used to identify the phases present. A possible overlap between the diffraction peaks makes this process more difficult. In a number of cases, also Rietveld analysis [141] is performed in order to extract quantitative information.

Macroscopic X-ray fluorescence (MA-XRF) imaging is a large scale variant of μ -XRF that has come in use since 2008 when it transpired that hidden/overpainted layers in paintings can be revisualized in this manner; significantly more (pictorial and chemical) information can be obtained than by means of X-ray radiography [142]. It involves the relatively fast scanning of a work of art relative to an X-ray source and XRF-detector assembly. Either the latter assembly is moved in front of the stationary artwork (mobile MA-XRF scanners) or vice versa. With typical dwell times of 50–200 ms per point, a (very) large number of XRF spectra (of the order of one to several million spectra/artwork) are recorded, yielding (after appropriate spectrum evaluation [143]) large-scale elemental maps (see Figs. 1c, 2b, c, 7c, d, 8, 9d, 10b). While its development started at a synchrotron facility [144], at which also the first studies were realized [142, 145–148], relatively soon mobile MA-XRF



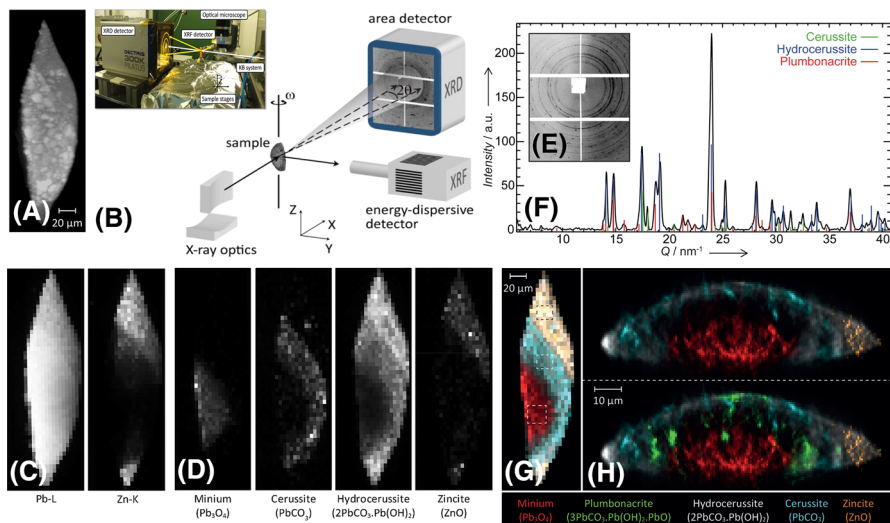


Fig. 4 **a** XRR image (obtained via X-ray absorption tomography) of a minium pustule removed from the surface of “Wheat stacks under a cloudy sky”, V. Van Gogh (Kröller-Müller Museum, Otterlo, the Netherlands). **b** Schematic and photograph of scanning XRF/XRD setup employed at Beamline P06 of PETRA-III. **c** XRF and **d** XRD 2D distribution images of the severed pustule (map size: 80 × 55 μm²). **e** 2D X-ray diffractogram of a plumbonacrite-rich location and **f** corresponding Q-space spectrum showing the peaks of various lead carbonates. **g** Color reconstructions of the projected and **h** the internal crystalline distribution of the paint sample. Pixel size: 45 μm² (in **c**, **d**, and **g**); 11 μm² (in **h**). Adapted from [163]

instruments were developed that allowed performing scanning experiments in the museum or picture gallery where the works of art are normally on display or are conserved [26, 149, 150]. With these MA-XRF scanners, it was possible to examine a great variety of artworks by well-known artists such as Rubens [22], Rembrandt [151–153], Vermeer [154], Goya [155], Van Gogh [145, 156], Magritte [157], Martins [158] and Pollock [159], and to discover new information on their artistic history and on their current state of conservation. Several X-ray instrumentation manufacturers and research institutions have recently described MA-XRF scanners of their own making [27, 160].

3 Multimodal X-ray-Based Identification and Degradation Studies of Artists’ Pigments

3.1 Pigments As Semi-Conductor Materials

Most of the artists’ pigments of which the spontaneous degradation behavior are described below are semiconductors. These are materials in which, upon absorption of photons, electrons can be promoted from the valence to the conduction band, leaving behind positive holes (see Fig. 5a). As illustrated in Fig. 5b, near the surface of the material, band bending can take place, which may lead to either electrons or

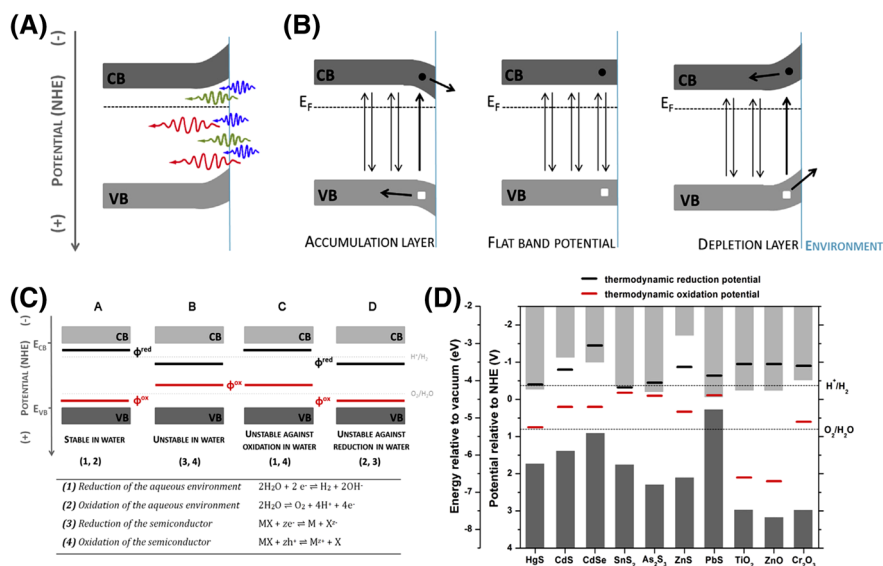


Fig. 5 **a** Indication of the penetration depth of blue (≈ 450 nm), green (≈ 510 nm), and red (≈ 650 nm) light. **b** Band bending for n -type semiconductors under illumination: accumulation layer (negative surface charge), flat band potential and depletion layer (positive surface charge, most common for n -type semiconductors). Arrows indicate either recombination of generated electron-hole pairs, or charge separation in the presence of an electric field induced by band bending. **c** Schematic overview on the stability of semiconductors in water. Oxidation and reduction potentials of a semiconductor relative to the oxidation and reduction potential of H_2O . **d** Oxidation and reduction potentials relative to the NHE and vacuum level for relevant semiconductor pigments or pigment degradation products in aqueous solution at pH 7 (pH 8.5 for ZnO), plotted versus the valence (dark grey columns) and conduction (light grey columns) band edge positions at pH 7. Adapted from [161]

positive holes being “injected” in the adjacent materials. The (in)stability of these pigments and the nature of the corresponding chemical transformations may be better understood/predicted by considering the positions of the valence band maximum (VBM) and conduction band minimum (CBM) in relation to their thermodynamic oxidation and reduction potential (ϕ_{ox} and ϕ_{red}) and that of water (see Fig. 5c) [161, 162]. In this manner, the positions of ϕ_{ox} and ϕ_{red} can be used for a fast screening of the stability of semiconductor pigments towards photo-induced corrosion in an aqueous/humid environment. This theoretical approach corresponds well with experimental data on pigment permanence and degradation phenomena found in the literature. By experimentally recording the photo-induced reduction or oxidation current emitted by the irradiated pigment/paint in an electrochemical setup that mimics the real environment of the degrading paint, the influence of potentially harmful environmental parameters (e.g., the wavelength and intensity of the exciting light, the type of solvent, its pH, the concentration of metal-binding ligands such as Cl^- and HCO_3^-) can be rapidly determined. It provides an experimental way of assessing whether or not a semi-conductor pigment is prone to photo-induced oxidation or reduction, with the advantage that it is much faster than more traditional approaches based on artificial ageing of paint model samples. Accelerated weathering experiments on such materials usually are time-consuming,

limiting the number of environmental factors of which the influence can systematically be examined. Moreover, during the long time period of artificial aging, the possibility exists that several chemical transformation processes (e.g. an initial photo-induced redox reaction followed by the precipitation of the released metal ions with suitable anions) may be taking place so that only their compound effect can be observed [163]. As concrete examples, the degradation behavior of the pigments cadmium yellow (CdS) and vermilion (α -HgS) were discussed in greater detail [162, 164, 165].

3.2 Pigment Degradation Studies Related to Fifteenth–Seventeenth Century Works of Art

Vermilion red (α -HgS) is a very frequently used semi-conductor pigment from the neolithic period onwards. It has been mined prehistorically and historically in China, Japan, Europe, and the Americas to extract metallic mercury (Hg^0) for use in metallurgy, as a medicine or preservative, and as a red pigment for (body) painting and in ceramics [166]. It is a pigment that features a complex multistep degradation pathway. Chlorine and sulfur K-edge μ -XANES investigation were combined with μ -XRD to determine the alteration mechanism that causes red pigment to acquire a grayish-black aspect (see Fig. 6) [167]. Paint fragments from Rubens paintings and from wall paintings in the Monastery of Pedralbes in Spain have also been examined [168–170]. Whereas elemental analyses of the degradation products revealed, along with mercury and sulfur, the presence of chlorine, XRD identified (in addition to α -HgS) calomel (Hg_2Cl_2) and the mercury-, sulfur-, and chlorine-containing minerals corderoite (α - $\text{Hg}_3\text{S}_2\text{Cl}_2$) and kenhsuite (γ - $\text{Hg}_3\text{S}_2\text{Cl}_2$). These observations are consistent with S- and Cl-edge XANES data. The resulting maps reveal a clear stratification between the primary mercury compounds (α -HgS) and the secondary species that arose from the interaction with environmental chlorine, leading the authors to hypothesize that α -HgS first takes up Cl, thereby converting into one or more $\text{Hg}_3\text{S}_2\text{Cl}_2$ phases. These light-sensitive compounds, following the loss of sulfur atoms, can be transformed into Hg_2Cl_2 , whereas sulfide ions oxidize into sulfate ions. The final step may involve the UV-induced disproportionation of Hg_2Cl_2 to HgCl_2 and may cause metallic mercury to turn white calomel into a grayish-black substance. No evidence for this transformation could be found with X-ray methods, although some relevant data were recorded via secondary ion mass spectrometry [171]. To study in greater detail the principle environmental factors (light, presence of halides) influencing the instability of red mercury sulfide and to better understand the chemical equilibria governing the formation and evolution of the different degradation compounds, a thermodynamic study of the Hg–S–Cl–H₂O system was made in combination with theoretical considerations and experimental ageing experiments [172]. The latter were performed in O₂-rich and O₂-poor circumstances (see Fig. 6d, e). From these it could be concluded that $\text{Hg}(0)$, α - $\text{Hg}_3\text{S}_2\text{Cl}_2$, and Hg_2Cl_2 can be formed from the reaction of α -HgS with $\text{ClO}(\text{g})$. Artificial aging experiments were carried out on model samples following the conditions assessed in the first part, in order to reproduce natural ageing observed on red mercury sulfide. Similarly to degradation compounds detected on original works of art, mercury



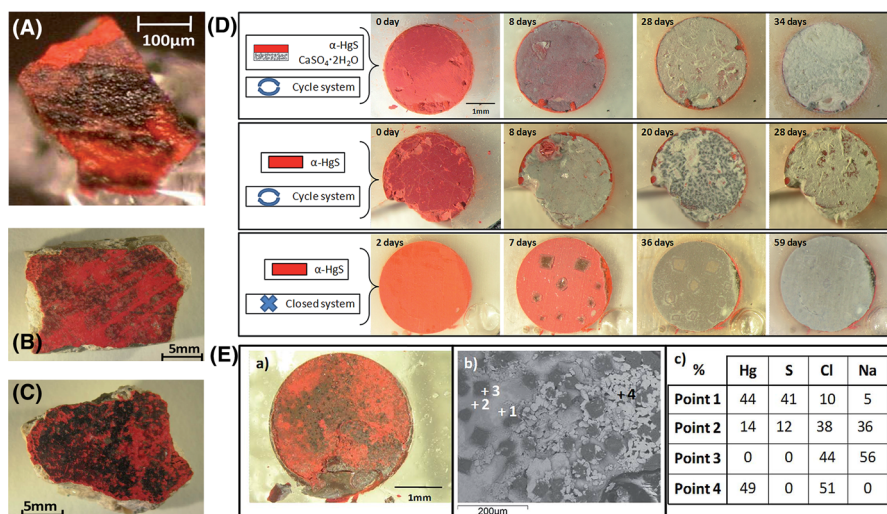
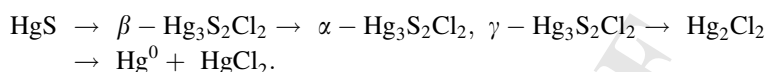


Fig. 6 Photographs of paint micro-fragments taken from: **a** *The Adoration of the Magi*, a painting by P. P. Rubens, Royal Museum of Fine Arts, Antwerp, Belgium; **b**, **c** a Roman fresco from *Villa delle Torre*, near Pompeii, Italy. **d** Pellets aged with NaOCl solution and light at different times of ageing: (*top panel*) two-layered vermilion/gypsum pellet, aged in a cyclic system; single-layered vermilion pellet, aged in (*middle panel*) cyclic and (*bottom panel*) closed system; **e** Visible and local backscattered electron (BSE) image of two-layered vermilion/NaCl pellet, aged with NaOCl in a closed system; the table shows quantitative SEM analyses results performed on the four points shown in the BSE image (in atomic percentage; Hg, S, Cl, and Na concentrations were normalized to a total of 100%; C, O, and Al data not shown here). Adapted from [170]

chlorine compounds such as calomel and corderoite were identified on the surface of α -HgS model samples when exposed to light and a sodium hypochlorite solution. Together with these compounds, sulfates were detected as well, and more particularly gypsum ($\text{CaSO}_4 \cdot 2\text{H}_2\text{O}$) when Ca was originally present in the model sample. These experiments also showed that light is a necessary factor to obtain degradation. From the relevant Pourbaix diagrams, it follows that both calomel and corderoite can be formed at basic pH, which is consistent with their formation in the presence of NaOCl solution (pH 12) during artificial aging experiments. These compounds appear to be formed simultaneously, but the visual aspect of the samples changed during the course of the ageing experiments, showing different steps and colors. In order to remain stable, corderoite needs chlorine to be always available as a reagent. In the case of aging in O_2 -rich circumstances, corderoite after some time disappeared and was converted into calomel. It, therefore, appears that corderoite is an intermediate product in the reaction of the formation of calomel from α -HgS. Mapping of cross-sections obtained from the artificially aged samples revealed a multi-layered structure similar to the ones observed on altered works of art, with mercury chloride compounds on top of red mercury sulfide layers and sulfates at the surface of the samples. Compounds containing both S and Cl are found in intermediate layers. Concerning the visual aspect of the degradation of red mercury sulfide, the different compounds detected on the pellets and on historical paintings (calomel, corderoite, kenh suite, gypsum) explain the observed white/purple colors,

but not the black one. The attribution of the black colour to meta-cinnabar (β -HgS) turned out to be unfounded. Theoretical spectroscopic results have indicated that none of the minerals identified as degradation compounds on mercury sulfide samples is intrinsically gray or black [165]. The presence of elemental mercury was proposed as a by-product of the photo-induced mechanism that causes the darkening of the paintings. In some conditions, the formation of Hg^0 from HgS is indeed thermodynamically favorable. By means of electrochemical methods [164, 173], the formation of metallic mercury from HgS by the joint action of light and chloride ions could be experimentally demonstrated. All the above consideration could be brought together in the following sequence of chemical transformations:



By means of a combination of laboratory-based experiments and thermodynamic modeling, the mechanism(s) and kinetics of cinnabar alteration in fresco applications was further clarified, specifically the role of light, humidity, and chlorine ions. Additionally, possible pathways and preventive and remedial conservation treatments during or immediately following excavation were explored to inhibit or retard darkening of cinnabar pigmented fresco surfaces [174].

Arsenic sulfide pigments (As_xS_y) are yellow (orpiment, As_2S_3) to orange-red (realgar, As_4S_4) p-type semi-conductors that have been used as wall painting pigments since antiquity, especially in Asia or Egypt [175, 176] and in illuminated manuscripts [177–179]. They have been used less extensively in Europe where less toxic or easier-to-use alternatives, such as lead–tin yellow, lead chromate, or cadmium yellow, were available and preferred. Nonetheless, both orpiment and realgar are frequently found in easel paintings, especially during the Venetian renaissance era and in still life or portrait details [180]. It is not also uncommon to find them in sculptures or decorative art objects [181]. Their sensitivity to light and resulting photo-oxidation in works of art is well described and often identified [182–184]: realgar (α - As_4S_4 , monoclinic, red) first becomes para-realgar (β - As_4S_4 , monoclinic, yellow) which then turns into arsenolite (As_2O_3 , white) while orpiment (As_2S_3 , yellow-gold) directly turns into arsenolite [176, 180, 182, 185, 186]. In oil paintings, the chemical degradation of emerald green ($\text{Cu}(\text{C}_2\text{H}_3\text{O}_2)_2 \cdot 3\text{Cu}(\text{AsO}_2)_2$) and of arsenic sulfide pigment have arsenic trioxide (As_2O_3) as a common degradation end product. In such paintings where this degradation takes place, arsenic is no longer confined to the pigment particles, but is detected via elemental X-ray analysis throughout the whole paint system, e.g., at layer interfaces, in varnishes, around iron- and aluminium-containing particles, and in the wood structure of a panel painting. The migrated arsenic is thought to be transported within the paint system as arsenic trioxide in aqueous form (H_3AsO_3) by the same mechanism as its transport in groundwater in the environment. In environmental studies, the oxidation of As(+III) to As(+V) is well documented; dispersed arsenic in paintings released from degraded pigments can, therefore, be a marker for water-linked transport processes [180]. In a cross section from *A Stone Cartouche with a Garland of Flowers* (1655) by the Flemish seventeenth century painter Daniel

Seghers (1590–1661), a combination of FTIR and Raman microscopy and XANES investigations was employed to identify and image the two oxidation states of the arsenic sulfide pigment and its secondary compounds—arsenite [As(+III), undegraded] and arsenate [As(+V), degraded]. This painting presented unquestionable signs of alteration as the yellow roses, originally painted using a mixture of arsenic sulfide and ochre, became transparent over time. The As-K edge μ -XANES spectra and maps collected from the cross section left no doubt that As(+V) compounds are effectively present while some of the corresponding Raman data are consistent with this [187]. Some indications are already available that the mineral schultenite (PbHAsO_4) can be formed in situ; a positive identification of this degradation compound by means of XRD could be realized in several seventeenth century paintings by J. De Heem (unpublished data).

Smalt was commonly used as a pigment by artists between the sixteenth and eighteenth centuries. It is a powdered blue potash glass colored by cobalt ions that easily degrades in oil paint, causing sometimes dramatic chromatic changes in the appearance of oil paintings. In many cases, reflection light microscopy demonstrated the presence of partially discolored smalt particles with a remaining blue core [188] (for an example, see Fig. 9b, c). The composition of smalt can vary considerably depending on the manufacturing process and the elements that are present in the raw materials in addition to the essential glass components silica, potassium oxide, and cobalt. It is known from historical documentary sources that smalt was available to artists in various grades with different color intensities, but it can be difficult to distinguish between pigment that is degraded and that which has always been rather grey in hue. Quantitative analysis of smalt pigment by SEM-EDX has proved to be a useful method of distinguishing between deteriorated and well preserved pigment based on the potassium content [189]. A typical pattern was encountered in a sample from Paolo Fiammingo's *The Sons of Boreas Pursuing the Harpies* (National Gallery London, NG 5467) [190]. In the upper layer of the cross section, where the smalt is mixed with lead white, it is well preserved and contains around 13–14 w% K_2O . The smalt in the lower layer, which was mixed with only a little lead white, is degraded: the paint appears yellowish; the pigment has lost its color almost entirely and contains only 1–2% K_2O . In order to investigate the changes in the structure and environment around the cobalt ion on deterioration and to further the understanding of the basis of the loss of color, particles of well-preserved and altered smalt in micro-samples from paintings in the National Gallery, London, and the Louvre Museum, Paris, were analyzed using XAS at the Co K-edge [191]. XANES and EXAFS measurements showed that in intense blue particles, the cobalt is predominantly present as Co(+II) in tetrahedral coordination, whereas in colorless, altered smalt the coordination number of Co(+II) in the glass structure is increased, and there is a shift from tetrahedral toward octahedral coordination. The extent of this shift correlates clearly with the alkali content, indicating that it is caused by leaching of potassium cations, which act as charge compensators and stabilize the tetrahedral coordination of the cobalt ions that is responsible for the blue color. The same samples were analyzed complementarily by using vibrational techniques such as μ -RS and SR-FTIR microscopy [192]. Comparison of the resulting spectra with those from modern smalt, together with



spectral decomposition and correlation with quantitative SEM-EDX analysis, shed new light on the role of the various cations in the silicate structure. Important modifications in the structure of the pigment on alteration were revealed, in particular the leaching of alkali ions and the formation of silanol groups, which subsequently condense to create new bridging Si–O–Si bonds and molecular water in the glass. The degradation mechanism and progressive deterioration of smalt were reproduced while also a theoretical explanation for the connection between the discoloration process and structural atomic changes around the Co atom was provided [193].

From antiquity, the pigment ultramarine was prepared by grinding the semi-precious stone lapis lazuli into powder. It was one of the most expensive artists' pigments throughout history. Lapis lazuli is composed of various minerals, among which aluminosilicates of the sodalite group. The most notable is the mineral lazurite $(\text{Na,Ca})_8(\text{Al}_6\text{Si}_6\text{O}_{24})(\text{SO}_4,\text{S,Cl})_2$ in which the cations and anions are trapped within the aluminosilicate framework. The pigment obtains its color from the fact that S_2^- and S_3^- anions are present inside the sodalite β -cages. Evidence of entrapment of carbon dioxide in the natural pigment from Afghanistan was found by Miliani et al. [194], indicated by the absorption band at 2340 cm^{-1} and a low frequency satellite corresponding to the $^{13}\text{CO}_2$ isotopologue. The thermal behavior of natural ultramarine was studied by FTIR, UV–vis spectroscopy, and XRD, from 300 to 1120 K. Measurements showed that CO_2 and the encapsulated S_3^- chromophore behave in the same way during the heating experiment, starting to be released only at about 670 K when the apertures of the sodalite β -cages became larger as an effect of temperature. The absorption at 2340 cm^{-1} can be used as a reliable discriminant between Afghan (the most probable source prior to the nineteenth century for Western artworks) and artificial ultramarine, a fact of great interest when dealing with the authentication of artworks. Recently, the possibility was investigated to distinguish lapis lazuli of difference geographic provenance based on their S–K edge XANES spectrum [195]. All examined lapis lazuli samples feature a S-XANES profile consistent with S_3^- being the dominant species (which considered to be the main responsible for the blue colour); however, also indications for the presence of species such as S_4^{2-} , S_4^- , and S_8 are apparent, depending on the origin of the material. However, the heterogeneity of the natural rocks hampers the straightforward association of one specific S K-edge XANES spectrum to a region of provenance. The blue pigments used on altarpieces in the fifteenth century in Catalonia and Crown of Aragon are principally composed of the mineral azurite. To a lesser extent, lapis lazuli was used and occasionally in the background areas and for outlining the principal figures; indigo (of vegetal origin) was used for the chromatic preparation layer. Data from several altarpieces belonging to well-known artists of that time were analyzed by SR-XRD, benchtop FTIR and SR-FTIR microscopy, RS, and SEM-EDX. XRD and SR-FTIR proved to be especially useful. The application of several layers with decreasing particle size, starting with azurite and finishing with lapis lazuli relates these artworks van Eyck's "Adoration of the Mystic Lamb" [196]. Synthetic ultramarine shares many properties with its natural form. Both natural and synthesis ultramarine have long been considered to be highly stable to light and compatible with other pigments. With both pigment forms, in



some circumstances, a grey-black to greyish/yellow discoloration of ultramarine-containing paint may be observed. In historic paintings, this phenomenon is known as “ultramarine disease” and is generally attributed to a break-up of the binding medium. In a recent study on color changes resulting from the interaction of various inorganic pigments with acrylic binding media under UV irradiation, ultramarine blue was found to have a very significant influence on alkyd resin paint, including a loss of blue color [197]. The opening of the sodalite cages of ultramarine [198] can cause its chromophoric S-anions to be released, leading to a loss of color of the pigment itself. Recently, Al-K edge XANES was employed to investigate the white discoloration of synthetic ultramarine in twentieth century paintings [199]. In degraded areas (induced by exposure during 1 min to 3 M HCl), the Al K-edge XANES featured an additional peak, corresponding to octahedral, six coordinated aluminium; in undegraded ultramarine, only the signature from AlO_4 units, part of intact β -cages, are observed. From this difference, it may be possible to conclude that the degradation of ultramarine may involve the removal of Al from the aluminosilicate network.

3.3 Alteration of Late Nineteenth/Early Twentieth Century Artists' Pigments

Below, we describe a number of recent case studies where a combination of X-ray and vibrational spectromicroscopic methods, sometimes together with more conventional laboratory-based analysis techniques, was used to shed light onto the degradation mechanism of pigments employed by artists such as James Ensor, Henri Matisse, Vincent van Gogh, and contemporary artists. The degradation behavior of various yellow pigments such as chrome yellow (PbCrO_4 or $\text{PbCr}_{1-x}\text{S}_x\text{O}_4$ with $x \leq 0.8$), zinc yellow ($\text{K}_2\text{O} \cdot 4\text{ZnCrO}_4 \cdot 3\text{H}_2\text{O}$), cadmium yellow ($\text{CdS}/\text{Cd}_{1-x}\text{Zn}_x\text{S}$), and Naples yellow [$\text{Pb}(\text{SbO}_3)_2 \cdot \text{Pb}_3(\text{Sb}_3\text{O}_4)_2$] were investigated by means of μ -XAS and/or related methods, in addition, the degradation of minium (aka red lead, Pb_3O_4) and Prussian blue [$\text{MFe}^{\text{III}}[\text{Fe}^{\text{II}}(\text{CN})_6] \cdot x\text{H}_2\text{O}$, with $\text{M}=\text{K}^+$, NH_4^+ , or Na^+].

To elucidate the reasons for the darkening of the originally bright chrome yellow (CY) paint in works by Van Gogh (see Fig. 2), a combination of μ -XRF, S, and Cr K-edge μ -XANES together with scanning transmission electron microscopy coupled to energy electron loss spectroscopy (STEM-EELS) was employed [156, 200–207]. This alteration proved to be caused by the surface reduction of Cr(+VI) to Cr(+III), but was very hard to document in a convincing manner using a combination of electron microscopy, Raman, and FTIR spectromicroscopies only. In samples taken from various paintings and in artificially aged CY paint of that period, Cr(+III) species were found, usually at the boundary between the paint and varnish layers and in sulfur-rich areas (see Fig. 2h). μ -XANES profiling and mapping (Fig. 2e–g) allowed the determination of the superficial brown coating that is 2–3 μm in thickness and contains non-crystalline Cr(III) compounds such as $\text{Cr}_2\text{O}_3 \cdot 2\text{H}_2\text{O}$, $\text{Cr}_2(\text{SO}_4)_3 \cdot \text{H}_2\text{O}$, and/or $(\text{CH}_3\text{CO}_2)_7\text{Cr}_3(\text{OH})_2$ [200]. The high sensitivity towards darkening of this material could be traced back to the presence of monoclinic and/or orthorhombic $\text{PbCr}_{1-x}\text{S}_x\text{O}_4$ ($0 \leq x \leq 0.8$) co-precipitate phases that are less stable than monoclinic (S-free) PbCrO_4 [203–208]. A change from the



monoclinic to the orthorhombic structure is observed in $\text{PbCr}_{1-x}\text{S}_x\text{O}_4$ when x exceeds 0.4 [202, 208].

To gain a deeper understanding of the behavior of the different types of chrome yellows, a series of oil paint models was prepared and characterized using a variety of methods before and after photochemical aging. The materials were obtained by employing commercial and in-house synthesized powders of PbCrO_4 and $\text{PbCr}_{1-x}\text{S}_x\text{O}_4$ co-precipitates with different x values [202, 203]. Also, samples of 100-year-old commercial paint were subjected to aging and the resulting differences investigated at the micro- and nanoscale [207]. In parallel, a large series of around 20 original chrome yellow paint samples, taken from paintings by Vincent van Gogh and some of his contemporaries were characterized [202]. By combining the results obtained from paint models and original paint samples, a number of conclusions could be reached:

- (a) Among the aged model oil paints, only those composed of a sulfate-rich orthorhombic $\text{PbCr}_{1-x}\text{S}_x\text{O}_4$ co-precipitate showed a significant darkening after photochemical aging. Cr K-edge μ -XANES investigations the formation of up to about 60% of Cr(+III) species in the outer layer of the most altered sample [203]. On the contrary, negligible alteration effects were observed when sulfate species (such as PbSO_4 and BaSO_4) were absent from the crystalline structure or were merely mechanically mixed with the original chrome yellow pigment. Only when the sulfate ions are inside the lead chromate crystal structure itself, the darkening phenomenon was apparent. This finding is attributed to a difference in solubility of the chromate compounds that becomes higher when their crystalline structure changes from monoclinic to orthorhombic [203]. By means of XRD, RS, and FTIR, it is possible to make clear the distinction between the different above-mentioned forms of chrome yellows [202, 208].
- (b) an evaluation of the influence of the wavelength (range) of UV–visible light on the photochemical reduction of the lead chromate-based pigments was also performed. Light-sensitive sulfur-rich/orthorhombic $\text{PbCr}_{1-x}\text{S}_x\text{O}_4$ ($x \sim 0.75$) co-precipitate was exposed to ranges of UV ($240 \leq \lambda \leq 400$ nm), UVA-VIS ($\lambda \geq 300$ nm), blue ($335 \leq \lambda \leq 525$ nm), and red ($\lambda \geq 570$ nm) light [203]. These experiments demonstrated that it is possible to slow down the darkening of this material by minimizing its exposure to wavelengths shorter than about 525 nm.
- (c) The above-mentioned forms of chrome yellow (both stable and less stable) were identified on about 20 embedded paint micro-samples originating from paintings by Van Gogh and some of his contemporaries. It was also possible to demonstrate that the identification of these different forms of chrome yellow is possible by carrying out non-invasive in situ analyses, i.e., by employing portable Raman and FTIR instrumentation. For example, in Van Gogh's paintings *Portrait of Gauguin* (Van Gogh Museum, Amsterdam, the Netherlands) and *Falling Leaves* (Les Alyscamps, Kröller-Müller Museum) the presence of the more light-sensitive $\text{PbCr}_{1-x}\text{S}_x\text{O}_4$ type of chrome yellow could be identified [202, 208].



By means of EELS, nanoscale maps of Cr(+VI), Cr(+III), and S(+VI)-containing species before and after light exposure of a historical light-sensitive chrome yellow paint were obtained [207]. This allowed a relatively simple degradation model to be proposed. Considering that this paint originally consists of nanograins of PbCrO_4 , $\text{PbCr}_{1-x}\text{S}_x\text{O}_4$, and PbSO_4 fixed in a porous network of cross-linked oil-based binder in which micro droplets of aqueous solution can be present, this model assumes that the degradation starts via an initial dissolution of CrO_4^{2-} ions into the aqueous phase. In their turn, these ions can react with the organic binder (oil) at those locations where the binder network and the water phase are in contact, thus oxidizing the binder material; this results in a reduction of the chromate ions to Cr(+III) compounds. The redox reaction is followed by precipitation of Cr_2O_3 as nanometer-thin outer layers on the surface of all particles that are present. Because of the leaching of chromate ions from the particles, several core-shell structures can be formed in situ on/in the particles.

An integrated approach based on a combination of diffuse reflectance UV-VIS, SR μ -XRF/ μ -XANES, and electron paramagnetic resonance (EPR) spectroscopies was used to study the photo-redox process in chrome yellows under the influence of monochromatic light of different wavelengths and several white light sources [205]. EPR spectroscopy was used as a complementary tool to SR-based X-ray methods due to its sensitivity for revealing species containing one or more unpaired electrons and for distinguishing different coordination geometries of paramagnetic centers, such as Cr(+V)-species. Semi-quantitative indications about the darkening of the paint surface were obtained by UV-VIS spectroscopy. The Cr speciation data highlighted that the reduction process was favored not only by (blue) wavelengths in the 400–460 nm range (i.e., where the pigment shows its maximum absorption), but also by (green) light in the 490–530 nm range. The first evidence of the presence of Cr(+V)-intermediates in the $\text{Cr}(+\text{VI}) \rightarrow \text{Cr}(+\text{III})$ reduction reaction was also gathered; this allowed the risks of inducing photo-degradation of the 490–530 nm wavelength range to be explained.

In order to distinguish between the transformations induced by specific relatively humidity (RH)/temperature conditions (i.e., >50% RH and a fixed temperature of 40 °C) and exposure to light, monoclinic PbCrO_4 , and orthorhombic $\text{PbCr}_{0.2}\text{S}_{0.8}\text{O}_4$ were subjected to separate or combined thermal and photo-chemical ageing protocols [206]. Diffuse reflectance UV-VIS and FTIR spectroscopies were used to obtain information associated with chromatic changes and the formation of organo-metal degradation products at the paint surface in combination with the above-mentioned Cr-speciation techniques. Under the thermal aging conditions employed, Pb(+II)-carboxylates and reduced Cr-compounds (in abundance of up to about 35% at the surface) were identified in the lead chromate-based paints. The tendency of chromates to become reduced increased with increasing moisture levels and was favored for the orthorhombic $\text{PbCr}_{0.2}\text{S}_{0.8}\text{O}_4$ compound. In the case of thermally aged paint models, a higher relative abundance of Cr(+V)-species were observed than in the case of the equivalent photo-degraded material where mainly Cr(+III) species were encountered. In paint models first subjected to a thermal treatment and then exposed to light, compounds ascribable to the oxidation of the organic binder were detected for all chrome yellow types investigated; however, the initial thermal



treatment increased the tendency toward photo-reduction of the $\text{PbCr}_{0.2}\text{S}_{0.8}\text{O}_4$ pigment only. For this light-sensitive compound, the variation in thickness of the photo-altered layer (containing ca 70% of reduced forms of Cr) as a function of moisture levels could be attributed to a surface passivation phenomenon taking place prior to photochemical aging.

Three micro-samples from two varnished paintings by Van Gogh and a waxed low relief by Gauguin (all originally uncoated) were examined with the aim of better understanding whether or not the application of the top coating influenced the morphological and/or physicochemical properties of the chrome yellow paint underneath [204, 209]. In all samples studied, regardless of the nature of the coatings (resins or wax), μ -XRF and Cr-K edge μ -XANES measurements showed that Cr(+III) alteration products were present in the form of grains inside the coating (generally enriched in S-species); the Cr(+III) compounds were also homogeneously spread at the paint surface. Inside the coating and within the grains, the alteration compounds were present in abundance up to 70 and 100%, respectively, and were identified as Cr(+III)-sulfates and -oxides. The distribution of Cr(+III) species may be explained by mechanical friction caused by brush-application of the coating that picked up and redistributed superficially formed grains of secondary Cr-compounds, likely already present in the reduced state as result of the photodegradation process. On the basis of the study of varnished chrome yellow paint models, no evidence could be found of an actively Cr-reducing role of the varnish or of superficial S-species.

Firm evidence for the chemical alteration of chrome yellow pigments in Van Gogh's *Sunflowers* (Van Gogh Museum, Amsterdam; see Fig. 2) was recently presented [156]. Noninvasive in situ vibrational spectroscopic analysis at several spots on the painting was combined with SR-based μ -XRD, μ -Raman, and μ -FTIR investigations of two paint micro samples to reveal the presence of lightfast PbCrO_4 and light-sensitive $\text{PbCr}_{1-x}\text{S}_x\text{O}_4$ (with x approximately equal to 0.5). Cr(+III)-compounds, products of this degradation process, were found at the interface between the paint and the varnish (see Fig. 2h). Selected locations of the painting with the highest risk of color modification by chemical deterioration of chrome yellow were identified; see also Sect. 4 below.

The production records for lead chromate pigments present in the nineteenth century archive database of Windsor & NewtonTM (W&N) for the manufacture of their artists' materials, were recently systematically studied [210]. W&N produced essentially three pigment types: (a) lemon/pale chrome yellow, based on solid solutions of lead chromate and lead sulphate [$\text{Pb}(\text{Cr},\text{S})\text{O}_4$], (b) middle or pure monoclinic lead chromate (PbCrO_4), and (c) deep lead chromate that contains the latter admixed with basic lead chromate (Pb_2CrO_5), accounting for 53, 22, and 21% of the production, respectively. Production recipes for primrose yellow (4%) resulted in mixed crystals with a high percentage of lead sulphate. Each pigment type is characterized by only one or two main synthetic pathways; process variations reveal a systematic and thorough search for a high-quality durable product. A comparison of the chemical composition of pigment reconstructions with early W&N oil paint tubes showed that their records entitled "pale" and "lemon"



correlated with the pigment tubes labelled chrome yellow while the records “middle” and “deep” corresponded with the tubes labeled “chrome deep”.

Some of the properties of the chrome yellow varieties containing variable amounts of S have been examined by employing density functional theory (DFT) calculations in order to better understand their photo-degradation behavior [211]. The results show that the mixed $\text{PbCr}_{1-x}\text{S}_x\text{O}_4$ and the native PbCrO_4 share a similar electronic structure, although an energy up-shift of the conduction band is computed by both increasing the amount of sulfate and passing from the monoclinic to the orthorhombic phase. The calculations suggest that, when the degradation would be considered to be purely an electron-exchange phenomenon, the Cr(+VI) photo-reduction would more difficult for compounds with high sulfur concentration and an orthorhombic phase. In reality, however, the opposite is true. Thus, it is likely that the degradation is more strongly influenced by other factors, such as a different solubility and/or (nano-)morphology of the $\text{PbCr}_{1-x}\text{S}_x\text{O}_4$ materials. Another theoretical study attempts to answer the question whether or not the degradation of $\text{PbCr}_{1-x}\text{S}_x\text{O}_4$ is purely a surface phenomenon; also, the question whether the bulk properties of the sulfur-rich pigment material trigger the process is still open [212]. First-principles calculations were employed to investigate the role of sulfur in defining bulk properties such as structure, stability, and optical properties of the materials. The calculations support the hypothesis that an initial local segregation of lead sulfate could take place. This material would then absorb UV light, thus providing the necessary energy for subsequent reduction of chromate ions into the greenish chromic oxide. To date, no experimental evidence to support this was found.

The darkening of zinc yellow ($\text{K}_2\text{O} \cdot 4\text{ZnCrO}_4 \cdot 3\text{H}_2\text{O}$), as observed in *A Sunday at La Grande Jatte* (G. Seurat, 1884, Art Institute of Chicago, Chicago, IL, USA) was studied by a combination of EELS and Cr-K edge XANES on artificially aged model paint samples and on original micro paint samples [213, 214]. To observe changes, more corrosive circumstances that needed for chrome yellows were needed, involving a combination of SO_2 gas, 50/90% humidity and light. Next to Cr(+III) species also dichromate ions [containing Cr(+VI)] were found as degradation products.

Cadmium yellow ($\text{CdS}/\text{Cd}_{1-x}\text{Zn}_x\text{S}$) is another class of yellow pigments frequently employed in the early twentieth century by painters such as Henri Matisse, James Ensor, Edvard Munch, and Vincent van Gogh. Cd-based pigments share a common hexagonal wurtzite structure in which cadmium and sulfur can be partially substituted to generate ternary phases with a wide range of colors from pale yellow to deep red. Among them, in $\text{CdS}_{1-x}\text{Se}_x$ solid solutions, the substitution of sulfur by selenium decreases the valence-to conduction energy gap, hereby modifying the color toward orange and red tonalities. UV–VIS–NIR and Raman micro-spectroscopies have been used for investigating the composition of ternary $\text{CdS}_{1-x}\text{Se}_x$ solid solutions employed as artists' pigments [215, 216]. The goal was the determination of the solid solution stoichiometry of a series of Cd-containing paints, by exploiting the linear dependence of some absorption, emission, and scattering properties with the pigment composition. The high sensitivity of Raman spectroscopy to local compositional and structural heterogeneity permitted to formulate a hypothesis



about the possible presence of quaternary solid solutions based on the substitution of cadmium by zinc ($\text{CdS}_{1-x}\text{Zn}_x\text{S}_{1-y}\text{Se}_y$) in commercial pigments and by barium ($\text{CdS}_{1-x}\text{Ba}_x\text{S}_{1-y}\text{Se}_y$) in historical paints. By employing a combination of S K-edge μ -XANES and μ -XRD, it was established that the oxidation of the pigment cadmium yellow (α -CdS) to cadmium sulphate ($\text{CdSO}_4 \cdot \text{H}_2\text{O}$) (white/transparent) was the chemical transformation responsible for the loss of the bright yellow color in a painting by J. Ensor [217]. In a follow-up paper [218], the same authors discovered that another chemical pathway has given rise to the formation of an orange-grey superficial crust in a painting by Van Gogh called *Flowers in a Blue Vase* (1887, KMM), containing the grey/white mineral anglesite (PbSO_4) and cadmium oxalate. The chemical and physical alterations of cadmium yellow (CdS) paints in *Henri Matisse's Le bonheur de vivre* (aka *The Joy of Life*, 1905–1906, The Barnes Foundation, Philadelphia, PA, USA), shown in Fig. 3a, have been recognized since 2006, when a survey by portable X-ray fluorescence identified this pigment in all altered regions of the monumental painting. This alteration is visible as fading, discoloration, chalking, flaking, and spalling of several regions of light to medium yellow paint. Similar secondary Cd-compounds (see Fig. 3h), such as CdCO_3 , $\text{CdSO}_4 \cdot n\text{H}_2\text{O}$ (Fig. 3c–f), and CdC_2O_4 (Cd-oxalate) as found in the Ensor and Van Gogh paintings have been identified [219–221]. By using a combination of μ -XRF (Fig. 2g), 2D full-field XANES imaging (Fig. 2h), μ -XRPD (Fig. 3i), and FTIR imaging of the altered paint layers, the question was addressed what the roles of cadmium carbonates and cadmium sulfates are found in the altered paint layers [222]. These compounds have often been assumed to be photo-oxidation products, but could also be residual starting reagents from an indirect wet process synthesis of CdS. In thin sections of altered cadmium yellow paints from *Le bonheur de vivre* the distribution of various cadmium compounds confirms that cadmium carbonates and sulphates are photo-degradation products. On the other hand, in *Flower Piece* (1906, H. Matisse, The Barnes Foundation), the cadmium carbonates appear to be remnants of the CdS manufacturing process, where CdCO_3 is the starting reagent. By employing TOF–SIMS species-specific mapping of degraded paint samples, three categories of inorganic and organic components could also be co-localized throughout *i*: (1) species relating to the preparation and photo-induced oxidation of CdS yellow pigments, (2) varying amounts of long-chain fatty acids present in both the paint and primary ground layer, and (3) specific amino acid fragments, possibly relating to the painting's complex restoration history [223].

As of the 1840s, cadmium zinc sulfides were extensively employed by nineteenth and twentieth century artists. The direct band gap of CdS is 2.42 eV, but can be modulated by the progressive substitution of Cd with Zn, resulting in pale yellow cadmium zinc sulfide pigments. Rosi et al. developed an analytical methodology for the non-destructive identification of different forms of yellow $\text{Cd}_{1-x}\text{Zn}_x\text{S}$ solid solutions based on electronic and vibrational spectroscopies such as XRF, μ -RS, reflection mode UV–VIS–NIR, VIS–NIR emission spectroscopy, and XRD. Six commercial CdS-based pigments and four historical pigments from the early twentieth century were examined. The reflection behavior in the VIS range and the emission profiles in the VIS and NIR ranges reflected the pigment composition while μ -RS allows to monitor the short range disorder in the CdS lattice caused by



Zn substitution. Information on the stoichiometry of the solid solutions and on their local structure could be obtained via XRD and by employing different Raman on/off resonance excitation conditions [215].

Minium or red lead (Pb_3O_4) is another frequently employed pigment employed by Van Gogh and contemporary artists. This orange–red pigment has been used since Antiquity. It contains both Pb^{2+} and Pb^{4+} -ions and has sometimes been observed to lose its red color. These transformations are either described as darkening of the pigment caused by the formation of either plattnerite ($\beta\text{-PbO}_2$) or galena (PbS) or as whitening by which red lead is converted into anglesite (PbSO_4) or (hydro)cerussite ($2\text{PbCO}_3\cdot\text{Pb(OH)}_2$; PbCO_3). By examining a degraded paint sample from Van Gogh's *Wheat Stacks under a Cloudy Sky* (1889, KMM) by means of conventional 2D and tomographic XRPD, it was possible to elucidate the degradation mechanism of minium and identify a missing link compound [163]. The degradation process was understood to be induced by absorption of 550 nm (or shorter) wavelengths, promoting electrons from the valence to the conduction band of minium. These electrons may reduce Pb(IV) to Pb(II) . The in situ formed Pb^{2+} (perhaps in the form of PbO) then captures CO_2 (either atmospheric or the result of oxidation of the paint binding medium) to form various lead carbonates. Next to the frequently encountered cerussite and hydrocerussite, a very rare lead mineral, plumbonacrite ($3\text{PbCO}_3\cdot\text{Pb(OH)}_2\cdot\text{PbO}$), was revealed to be present. The location of this compound was revealed via XRPD-tomography (Fig. 4b) of a hemispherical paint protrusion, at the centre of which a partially degraded grain of minium was present (see Fig. 4g, h). Evidence for the presence of a series of consecutive equilibria, gradually transforming plumbonacrite into cerussite via hydrocerussite was found. In a follow-up paper, the influence of several parameters on the tendency towards degradation of minium such as (a) a surplus of PbO inside the red lead material itself, (b) the pH, and (c) the concentration of available HCO_3^- or CO_3^{2-} -ions was investigated [224]. For demonstrating the photoactivity of the pigment, an electrochemical setup with a minium-modified graphite electrode (C 1 Pb_3O_4) was used. It could be confirmed that minium behaves as a *p*-type semiconductor, photoactive during illumination, and inactive in the dark. Raman measurements confirm the formation of degradation products. The photo-activity of the semiconductor pigment is partly defined by the presence of PbO impurities; these introduce new states in the original band gap. It was experimentally evidenced that the presence of PbO particles in minium leads to an upward shift of the valence band, reducing the band gap. Thus, upon photoexcitation, the electron/hole separation is more easily initialized. The $\text{PbO/Pb}_3\text{O}_4$ composite electrodes demonstrate a higher reductive photocurrent compared to the photocurrent registered at pure PbO or Pb_3O_4 -modified electrodes. In the presence of bicarbonate ions, a significantly higher photoreduction current is recorded because the PbO that is formed in situ reacts further to become hydrocerussite. It could be shown that the presence of bicarbonates in the environment stimulates the photodecomposition process of minium and plays an important role in the degradation process.

The fading of modern pigments based on Prussian blue blues $[\text{MFe}^{\text{III}}[\text{Fe}^{\text{II}}(\text{CN})_6]\cdot x\text{H}_2\text{O}]$, with $\text{M}=\text{K}^+$, NH_4^+ or Na^+ , another class of pigments frequently employed by Van Gogh [2] and other artists [69, 225], in the presence of various



white pigments has also been investigated [138, 226–230]. Painted samples were studied by UV–VIS, Fe K-edge X-ray absorption, ^{57}Fe transmission Mössbauer spectroscopy, and attenuated total reflectance (ATR) infrared spectroscopy. XAS revealed an effective decrease in the iron coordination number in the aged samples, which, combined with Mössbauer data, suggest a reduction of the surface iron ions in the Prussian blue upon exposure to light.

4 State-of-the-Art X-ray-Based Chemical Imaging of Painted Works of Art

4.1 Macroscopic X-ray Fluorescence Imaging (MA-XRF)

In a number of recent papers, the results obtained via MA-XRF were compared to those obtained by other methods providing elemental distribution information on the square meter scale. Next to XRR, also neutron activation autoradiography (NAAR) provides information of this kind [231]. Given the differences between XRR, MA-XRF, and NAAR in the fundamental physical phenomena exploited, a theoretical comparison of their capabilities is not straightforward and critical comparisons of their use on the same painting were not available until recently. While NAAR images tend to be more difficult to interpret because they usually contain contributions from more than one element/pigment, MA-XRF maps provide more direct and intuitive information on the distribution of pigments. The different mechanism by which the images are created also affects the sharpness of the resulting image. In NAAR, for example both the copper and mercury radionuclides produce high-energy radiation. In the case the photographic film not in direct contact with the paint, the path the electrons must bridge between paint and film can cause cause blurring of the NAAR images. By contrast, MA-XRF images that are obtained by scanning can be much sharper in such cases. However, the absorption of characteristic XRF radiation emitted by elements in underlying paint layers by overlying strata may significantly influence the maps.

During the investigation of Rembrandt's painting *Susanna and the Elders* (Gemäldegalerie, Berlin, Germany), XRR, NAAR, and MA-XRF data were juxtaposed [232]. In the XRR images, which are dominated by the Pb distribution, many pentimenti (i.e., intentional changes to the composition, made by the original artist) are visible, but given the complex genesis of the painting, their identification in the radiograph was not straightforward. The painting features a considerable number of overpainted features and a wide range of pigments with different elemental tracers, including earth pigments (Mn/Fe), azurite (Cu), lead white (Pb), vermilion (Hg), and smalt (Co, As) are present. MA-XRF suffers from few spectral overlaps and the scanning of the painting was performed in a few tens of hours and in situ, i.e. in the museum itself. NAAR required the stay of the painting at a nuclear research facility for several weeks while inter-element interferences are more difficult to resolve. Moreover, only a limited number of elements contribute to the acquired autoradiographs, most notably Mn, Cu, As, Co, Hg, and P while highly relevant elements such as (K), Ca, Fe, and Pb do not show up in the NAAR images.



However, NAAR provides a higher lateral resolution and is less hindered by absorption in covering layers, which makes it the only method capable of visualizing P in lower paint layers. Comparison of the MA-XRF Pb and Hg distribution of *Susanna and the Elders* suggest, for example, that the first Elder's hand was repositioned several times.

Another painting by Rembrandt that was studied by both MA-XRF and NAAR is *An Old Man in Military Costume* (1630–31) in the J. Paul Getty Museum (Los Angeles, CA, USA) [151]. The objective of the study was to virtually reconstruct the hidden portrait below the one that is now visible. The challenge of reconstructing the overpainted figure in *An Old Man in Military Costume* was significantly advanced by the judicious combined use of imaging methods. XRR provided information on part of the face and the area of the eyes since it largely reflects the distribution of lead white. NAAR provided a strong image of the face and cloak of the underlying figure, along with an indication of the chemical composition. The single-element distribution maps produced by MA-XRF provided additional details into the shape of the underlying image and the composition of the pigments used. The underlying figure's face proved to be richer in mercury than the face of the figure on the surface. Likewise, the cloak of the underlying figure was found to be richer in copper than the surface figure although the nature of the copper-containing pigment could not be determined from these data. The use of iron earth pigments, specifically, Si-rich umbers, came forth from complementary information provided by the NAAR and MA-XRF maps; more specifically, the MA-XRF Fe distribution revealed the shape of the first portrait's gorget or collar. These data were used to create a false color digital reconstruction, yielding the most detailed representation of the underlying painting to date. This new reconstruction, and associated information on the pigments employed in both the upper and lower images serves to invigorate the art-historical discussion on the exact nature of the concealed figure and its significance in Rembrandt's oeuvre.

NAAR and XRF imaging were also used in the investigation of *The Reading Hermit* (1630), allegedly painted by Rembrandt [233].

Gradually, the elemental mapping capabilities of MA-XRF are being employed for the investigation of works of art other than oil paintings. Its applicability for investigating stained-glass windows inside a conservation studio was assessed by analyzing a well-studied late-medieval panel from the City Museum of Bruges (Belgium), showing Saint George and Saint Michael (see Fig. 7) [234]. Although accurate quantification of components is not feasible with this analytical imaging technique, plotting the detected intensities of K versus Ca in a scatter plot allowed distinguishing glass fragments of different compositional types within the same panel (Fig. 7c1–c4). In particular, clusters in the Ca/K correlation plot revealed the presence of two subtypes of potash glass and three subtypes of high lime-low alkali (HLLA) glass. MA-XRF results proved to be consistent with previous semi-quantitative SEM-EDX analyses on two glass micro-samples and theories on glass production in the Low Countries formulated in literature. A bi-plot of the intensities of the more energetic Rb-K versus Sr-K emission lines yielded a similar glass type differentiation and presented a suitable alternative in case the Ca/K signal ratio is affected by superimposed weathering crusts. The MA-XRF maps permitted the



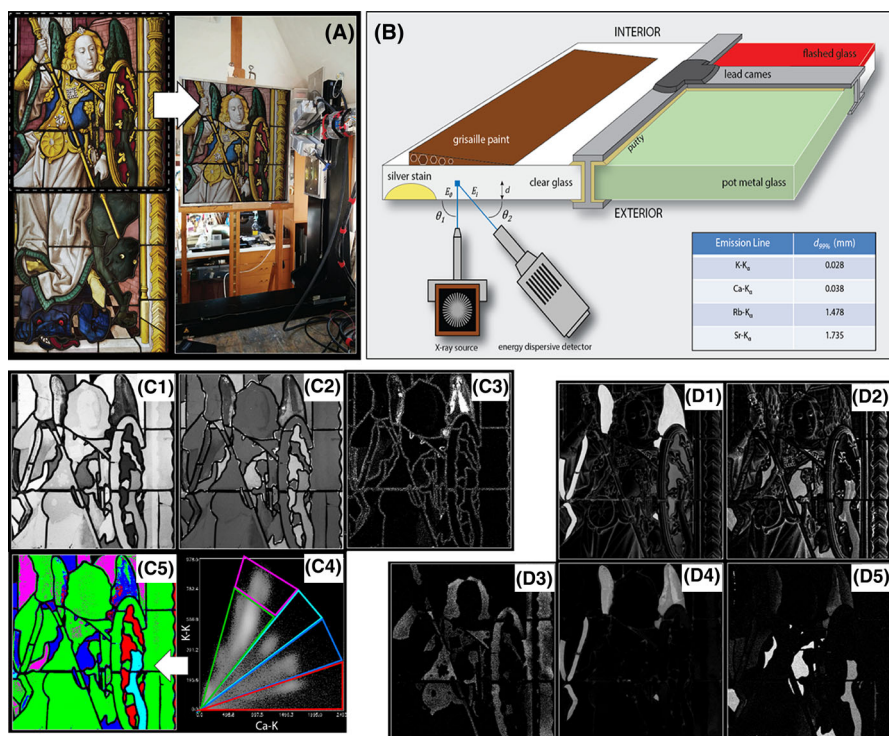


Fig. 7 Stained glass window from the collection of the City Museum of Bruges showing Saint Michael, dated ca. 1490, in front of the MA-XRF scanner; **b** schematic of build-up of a stained glass window and measurement geometry on interior side. The table lists sampling depths for different XRF energies; Elemental maps collected from the interior side: **c1** K, **c2** Ca, and **c3** S; **c4** Ca vs K-K_α intensity scatter diagram with pixels clusters indicated; **c5** Locations of color-coded pixel clusters. Elemental maps collected from the interior side: **d1** Cu and **d2** Co; from the exterior side: **d3** Ag, **d4** Cu, and **d5** Co. Adapted from [234]

1144 identification of the chromophores responsible for the green, blue and red glass
 1145 colors. In addition, by contrasting MA-XRF Maps from the interior with exterior
 1146 side of the window, it was possible to discriminate between glass panes made in
 1147 colored pot metal glass (i.e., glass that is colored throughout the pane) and those
 1148 made in multi-layered flashed glass (i.e., colorless glass covered with one or more
 1149 thin, intensely colored glass coatings). The benefit of obtaining compositional
 1150 information from the entire surface, as opposed to point analysis, was illustrated by
 1151 the discovery of what appears to be a green cobalt glass feature (see Fig. 7d) that
 1152 was previously missed on this well-studied stained-glass window, both by
 1153 connoisseurs and spectroscopic sample analysis. Generally, the major benefit is
 1154 the ability to acquire compositional data from the entire surface in a non-invasive
 1155 way. In addition, the ensuing chemical data can be presented in a visual way, hence
 1156 making their interpretation easier for non-XRF specialists. However, in contrast
 1157 with conventional SEM-EDX and μ -XRF point analyses on samples, MA-XRF
 1158 experiments do not provide accurate quantitative composition information on the
 1159 different glass components. Although essentially qualitative in nature, the resulting

insights are particularly useful for conservators who are typically interested in an efficient discrimination of the historical phases in one specific window rather than in the exact chemical composition of the different glass types present. The mobile aspect of the instrument allows performing the experiments directly inside a conservation studio and the ensuing elemental distribution maps can also serve as functional working drawings during the actual treatment. However, the lack of absolute concentration data of the various glass constituents does prevent inter-comparison of MA-XRF data obtained from different stained-glass windows. In this framework, combining the MA-XRF maps with SEM-EDX analyses on a limited number of samples is expected to be particularly relevant. Moreover, by creating MA-XRF maps, sampling locations for SEM-EDX investigations can be selected in a highly substantiated way. Thus, the number of micro samples required for obtaining a comprehensive compositional overview of the glass types present in a glass window can be minimized and the resulting sample data can be extrapolated to the rest of the glass surface in a more confident manner.

The benefits and limitations of employing MA-XRF for the study of manuscript illuminations were recently discussed [235]. As a representative example of this type of objects, a fifteenth century Italian manuscript fragment from the collection of the Fitzwilliam Museum in Cambridge (UK) was investigated. MA-XRF scanning of this fragment was undertaken to gain insight into the materials and techniques of Renaissance illuminators and to help answer specific questions regarding its authorship and place of execution, currently considered to be either Bologna or Rome. The non-invasive analysis permitted to reconstruct the palette employed by the anonymous illuminator and highlighted the likely use of two unusual pigments: an arsenic sulphide glass and a manganese (hydr)oxide. Identification of the latter would have been difficult without an elemental Mn map, which showed no overlap with the Fe distribution, excluding the presence of umber pigments, widely used and, therefore, less distinctive of a specific artist or school. The use of manganese oxides as black pigments as hitherto been identified almost exclusively in easel paintings by a number of sixteenth century artists working in northern and central Italy, such as Perugino, with whom the unknown artist of the manuscript fragment shows stylistic affinities. Although MA-XRF could not provide a definite answer to the question of geographic origin, this kind of analysis did offer strong support to securely place the fragment within a specific artistic milieu. In order to realize a more precise and more reliable pigment identification on these type of artefacts, MA-XRF scanning is best combined with a series of RS or XRD point measurements.

MA-XRF was used together with optical coherence tomography (OCT) for the inspection of a late sixteenth century illuminated parchment manuscript (a gradual), originating from the Convent of the Benedictine Sisters in Lviv (Ukraine) (Fig. 8) [236]. It was employed both for mapping the elemental distribution over large parts of the folios (which included illuminated initials; see Fig. 8a–d), for quantitative analysis of the composition of the smalt pigment, and for documenting changes in the composition of the iron gall ink on different pages. OCT, by providing cross-sectional images of painted details, helped to interpret the XRF results. Of the two non-invasive techniques, MA-XRF appeared to be the more useful. As opposed to



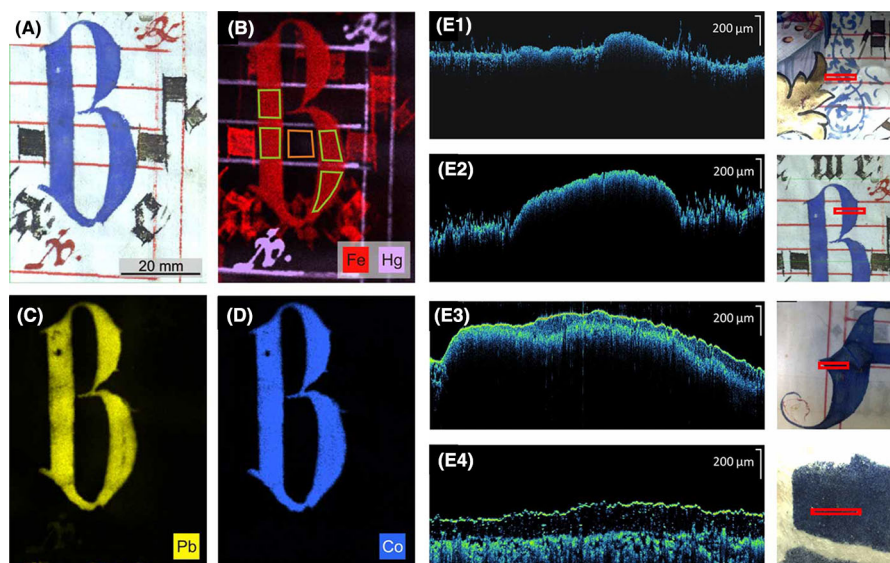


Fig. 8 **a** Optical photograph and elemental maps of **b** Fe, Hg, **c** Pb, and **d** Co a capital “B” from a sixteenth century gradual, originating from a Benedictine Convent (Lviv, Ukraine) **e** OCT profiles of several details of blue-lettering (red rectangles). Adapted from [236]

the local approach employed with PXRF, the ability of MA-XRF to scan large areas allows for a more general characterization of the object, not restricted to small regions of examination or to the collection of samples from them. OCT also yields images of relatively large structures; Fig. 8e shows virtual OCT cross sections of different locations on the manuscript. However, OCT suffers, due to the high scattering properties of historic parchment, from the drawback that the information retrieved is relatively limited.

4.1.1 Multi-Modal Investigation of “Christ with Singing and Music-Making Angels”, H. Memling

To illustrate the interplay between spectroscopic methods for non-invasive imaging, for point measurements and for microscopic pigment identification/imaging, their combined use for a full characterization of the fifteenth century work of art, *Christ with Singing and Music-Making Angels*, by Hans Memling was described [21]. This involved the recording of MA-XRF and MA-rFTIR maps (see Fig. 1), providing information on Memling’s painting and colour rendering technique. For example, vermilion red was used in the cloak embroidery and in the bright red parts of the wings of some of the angels, while at a lower concentration level, it was also present in the flesh tones of the faces. In the more purplish tones, madder lake was the major colorant, sometimes mixed with azurite. The latter pigment was also employed in all blueish areas. For the hair of the angels, clay-containing earth pigments (Fe, e.g. from goethite) were employed, with lead tin yellow for the highlights. The worn gilded background features high Au and reflected infrared signals but also Ca and Fe

signals, both of which originate from an underlying adhesive bole layer. In Fig. 1c, a composite of the relevant MA-XRF elemental maps is shown. In the examined areas, almost no indications of pentimenti were encountered.

4.2 Studies Combining Large-Scale Chemical Imaging and Microscopic Paint Sample Analysis

Next to the use of MA-XRF and related methods for subsurface visualization of overpainted representations, this chemical form of imaging of paintings is also increasing being used as part of pigment degradation studies. Below a number of investigations are described where macroscopic chemical imaging is combined with microscopic analyses of minute paint samples.

4.2.1 Identification and Localization of Different Smalt Types in “Saul and David”, Rembrandt

The painting “Saul and David”, shown in Fig. 9, is thought to date from c. 1652 and previously was attributed to Rembrandt van Rijn and/or his studio. It is a complex work of art, recently subjected to an intensive conservation treatment and associated investigation [153]. It was anticipated that its analysis would shed light on authenticity questions and Rembrandt’s role in the creation of the painting. The painting was thought to have been started in a colorful style characterized by great detailing and smooth handling of the paint. In contrast, the adjustments made to the painting during the second stage are painted very loosely; some scholars are in doubt whether this second stage was executed by Rembrandt—some of his assistants may have completed the work. It would seem that the painter was experimenting with the use of smalt in this second phase, since it was found over much of the painting, not only in the blue areas of the turban, which belong to the first phase. The extensive use of smalt, especially in mixtures with bone black, lakes, and earth pigments is considered typical of Rembrandt’s late painting technique. Its pigment combination was not only useful to create coloristic effects, but also for its drying properties and to give bulk and texture to the paint. As part of the investigation into the authenticity of the curtain area, a number of paint micro-samples were examined with light microscopy (LM) and SEM-EDX. Given that the earth, smalt, and lake pigments used in the painting could not be imaged with traditional imaging techniques, the entire painting was also examined with state-of-the-art non-invasive imaging techniques. Special attention was devoted to the presence of cobalt-containing materials, specifically the blue pigment smalt, considered characteristic for the Rembrandt’s late artistic production [152]. The painting and a selected number of MA-XRF distribution maps, recorded prior to removal of overpaint and darkened varnish layers, are shown in Fig. 9a, d, respectively. From the Fe and Co distribution maps, it is immediately clear that the upper right canvas piece (part γ) painted in a monochrome dark tone does not show the same origin as the canvas sections of *Saul and David* (parts α and β , respectively). Both Co and Fe appear to be present throughout the γ area at high abundance; the joins between the various sub-parts, as well as the entire γ -section



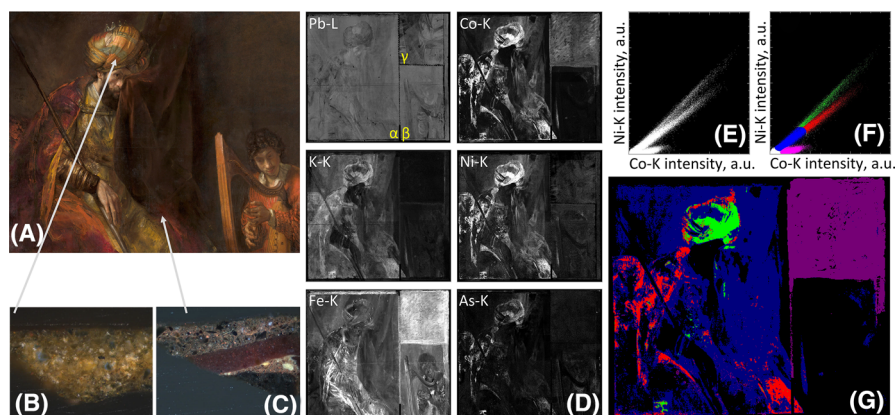


Fig. 9 *Saul and David* by Rembrandt, (c. 1652, 126 × 158 cm, Royal Museum Mauritshuis, Den Haag, the Netherlands, inv. no. MH621, oil on canvas); **b, c** Optical micrographs of two paint cross sections (locations indicated); **d** MA-XRF maps (1656 × 1311 pixels) of various elements present in the painting; **e** Ni-K vs. Co-K XRF intensity scatter plot; **f** as E, color codes: *green*: “high Ni”, *red*: “medium Ni”, *magenta*: “low Co/Ni”, *blue*: “rest”; **g** location map of color-coded pixels. Adapted from [152]

were uniformly covered with an Fe- and Co-containing paint in order to dissimulate the differences with sections α and β . The Co map of the α -section demonstrates that smalt was extensively used in the areas of the turban, the curtain, Saul's garments and his chair. K is associated with smalt, but also with red lake (likely from alum or KOH added during its production). The Fe-distribution in the α -section is quite different from the other elements since it is dominated by the earth pigment-containing areas, where the Fe concentration is much higher than in smalt (where it is of the order of a few wt%). The Co map has a patchy appearance at the left and bottom of the picture, areas corresponding to Saul's cloak, which initially appears to have extended over the chair. The lighter (higher intensity) areas in the Co map correspond to the thicker/more intact smalt-rich paint. Paint cross-sections (Fig. 9c) from the dark patchy areas in the scans of Saul's show the presence of an incomplete smalt-rich top paint layer applied on top of red lake glazes. The partial removal of the smalt paint from Saul's garment and chair is most likely due to a misinterpretation during a past restoration, where a restorer tried to recover the bright red color of Saul's cloak, obscured by a discolored and darkened smalt layer. In the Ni:Co correlation plot (Fig. 9e, f), the existence of smalt characterized by various distinct Ni:Co ratios is clearly visible. Next to the “medium Ni” group of pixels (labeled red in Fig. 9f), a smaller group of pixels (labelled green) is present characterized by a Ni:Co ratio that is ca. 25% higher than in the “medium Ni” group. This “high Ni” group of pixels is situated in Saul's turban and some small parts of his clothing. The “medium Ni” group of smalt pixels corresponds to patchy areas of paint of uneven thickness that are present in Saul's garment in sections α and β . The pixels belonging to the curtain area in the background between the figures of Saul and David, generally showing both a low Co and Ni intensity, were labelled blue. In magenta, a fourth group of pixels, characterized by a very low Ni to Co XRF intensity ratio is also visible in Fig. 9g, corresponding to the paint used to

cover the canvas insert γ [153]. Microscopic examination of paint samples from this section showed that Co is not present in the form of smalt pigment particles but in a more finely divided state, dispersed through the layer. The Co material was likely added to the nineteenth century overpaint as drying agent. In sections α and β however, the Co and Ni are definitely present inside coarsely ground smalt particles. The difference between the “medium Ni” and “high Ni” areas could also be found back in the quantitative SEM-EDX data of paint samples from both areas (shown in Fig. 9b, c). From analysis of a series individual smalt particles it was possible to infer that (a) the leaching process significantly decreases the K_2O content of the glass, typically from a level of 10–16 to 2–5 wt% while it does not seem to have a large effect on the observed NiO:CoO concentration ratio; (b) the two average NiO:CoO ratios obtained in both areas of the painting are significantly different at the 99% confidence level: the “turban area” particles on average show a mean NiO:CoO concentration ratio of 0.35 ± 0.06 (1 s) that is significantly higher than the average ratio of the particles in the “garment area” where it is 0.28 ± 0.07 . This observation is consistent with the MA-XRF scatter plots of Fig. 9e–g, were in the turban area, a Ni:Co intensity ratio that is ca. 25% higher than that in the garment area is observed. In this manner the combination of quantitative SEM-EDX analysis and MA-XRF scanning revealed that three types of Co-containing materials are present in the Saul and David painting.

4.2.2 Evidence for Pigment Degradation in “Sunflowers” by V. Van Gogh

The *Sunflowers* painting shown in Fig. 2 was painted by Vincent Van Gogh in Arles in 1888–89 as part of a series of seven, all depicting a bouquet of sunflowers in an earthenware pot. The extent to which spontaneously occurring color changes have influenced today’s outlook of the paintings has been questioned, while previous studies showed that CYs ($PbCr_{1-x}S_xO_4$ with variable sulfate content x) are prone to darkening due to (photo-)reduction. The formation of reduced Cr is more favored for sulfate-rich, lemon-yellow, orthorhombic $PbCr_{1-x}S_xO_4$ varieties of the pigment (with $x > 0.4$) than for the orange-yellow, monoclinic $PbCrO_4$ that is the most lightfast of these materials [200, 202, 203, 205, 206]. A combination of non-invasive methods such as MA-XRF, FTIR, and RS were performed in situ on the version of *Sunflowers* owned by the Van Gogh Museum (Fig. 2a). Microscopic investigation of minute paint samples was undertaken (1) to assess the extent to which the painting contains lightfast $PbCrO_4$ (henceforth denoted as LF-CY) and light sensitive S-rich $PbCr_{1-x}S_xO_4$ ($x > 0.4$) (LS-CY), and (2) to determine whether or not these pigments have been subject to a reduction process [156]. The MA-XRF maps of the painting (Fig. 2b, c) show that Pb and Cr are the main elemental constituents of the sunflower petals, the orange corollas and the table area. In the pale yellow background, Zn is the predominant element (Fig. 2b), suggesting the presence of zinc white (ZnO), while Pb and Cr are present in a significantly lesser quantities. In some of the ochre and orange tones of the sunflower petals, besides Pb and Cr, Hg, and/or Cu and As were also found (Fig. 2c), due to the presence of vermilion (HgS) and/or emerald green [$3Cu(AsO_2)_2 \cdot Cu(CH_3COO)_2$]. In areas of the sunflower petals and the upper region of the vase with no or very little Pb and Cr, Fe



is the main constituent element instead, indicating the use of a yellow ochre (Fe-hydroxide based pigment). All the above-mentioned pigments are frequently encountered in works by Van Gogh. In the green(ish) areas, besides Cu and As, Pb and Cr are sometimes found together too, suggesting the use of mixtures or overlapping brush strokes of emerald green and CYs. The Pb- L_{α} :Cr- K_{α} XRF intensity ratio changes throughout the painting (Fig. 2b), suggesting a distribution of different CY types. However, the presence of other Pb- and/or Cr-based pigments, also frequently used by Van Gogh, such as red lead (Pb_3O_4), lead white [$PbCO_3$, $Pb_3(CO_3)_2(OH)_2$], or viridian green ($Cr_2O_3 \cdot 2H_2O$), and variations of the paint thickness (giving rise to self-absorption of variable magnitude), could also cause a change in the Pb- L_{α} :Cr- K_{α} intensity ratio. No meaningful S-distribution maps could be recorded, mainly due to the spectral overlap between the S-K and Pb-M XRF signals and the limited MA-XRF sensitivity for these signals. More reliable insights into the distribution of the different types of CY were obtained by performing vibrational spectroscopic and structural analyses at a select number of points on the surface of the *Sunflowers* painting (see Fig. 2d for a summary of the results). In the light yellow table area, non-invasive Raman and reflection mid-FTIR analyses revealed the presence of LS-CY ($x \approx 0.5$). This finding was confirmed by SR-based μ -XRD and vibrational spectroscopic analysis of a sample from the region (F458/4). In the Zn-rich pale yellow background, Raman spectroscopy (Fig. 2d) again demonstrated the presence of LS-CY ($x \approx 0.5$). For the sunflower petals, various CYs appear to have been used. While in the light yellow areas, a type of LS-CY very similar to that detected in the table and background was identified by Raman spectroscopy, on the other hand, in the ochre-yellow petals, the presence of LF-CY (i.e., monoclinic $PbCrO_4$) was observed. Occasionally, this is mixed with LS-CY or red lead. Chrome orange and vermilion red are sometimes also present in the darker/orange petals. SR-based μ -XRD and μ -Raman mapping experiments of regions of interest of one of the studied paint samples (F458/1) confirmed the non-invasive analyses: LF-CY is the chief constituent of the orange-yellow shades, while LS-CY ($x \approx 0.5$) is the main phase in the lighter yellow hues. Clear indications for the gradual conversion of Cr(+VI) to Cr(+III) were found. Next to Cr(+III)-rich particles, Cr(+III)-species are present as a 2–3 μ m thick layer right at the varnish/paint interface. Here, the relative abundance of Cr(+III) is around 35%, decreasing to 0% when going deeper inside the yellow paint. This pattern is very similar to that previously observed in photochemically aged LS-CY ($x > 0.4$) paint models [200, 202, 203, 205, 206]. In summary, the non-invasive identification and macro-scale level distribution of the light-sensitive chrome yellow in the *Sunflowers* painting in combination with analysis of paint micro samples has permitted to identify selected locations with the highest probability/risk of color change due to Cr(+VI) reduction and to provide the first evidence on the conservation state of chrome yellow in selected regions of the painting.



4.2.3 Combining MA-XRF and VNIR Hyperspectral Imaging for the Study of *Le Portrait*, R. Magritte

Diffuse reflectance imaging spectroscopy can be used to separate and identify many artist pigments by virtue of their unique electronic transitions and vibrational features in the visible to reflective near infrared (400–2500 nm) [27, 157, 237–240]. When combined with MA-XRF scanning results, a more complete identification and mapping of artists' materials is possible [27].

“Le portrait” (*The Portrait*, 1935, The Museum of Modern Art (MoMA), New York City, NY, USA), shown in Fig. 10, is a painting by Belgian surrealist artist René Magritte (1898–1967). It is a classic example of Magritte's imagery, characterized by the realistic representation of ordinary objects made surreal by context or their relationship to each other. In the corresponding XRR image, an underlying composition is visible, showing the head and torso of a female nude. A similarity between the figure in the XRR image and the upper left quarter of a painting by Magritte entitled “La pose enchantée” (*The Enchanted Pose*), presumed lost, can be recognized. Preliminary in situ analyses by means of PXRF suggested the presence of a chromium based pigment in the sky and of an iron oxide based pigment in the darker areas of the female face. To gain a more thorough and overall depiction of the hidden layer, MA-XRF was used to identify and map the distribution of key chemical elements representative of pigments commonly found in artists' paintings, thus revealing information on the color palette employed by Magritte while painting “La pose enchantée”. Secondly, visible and near infrared (VNIR) hyperspectral imaging was performed to complement the information obtained by XRR and MA-XRF, both with respect to the hidden figure and to Magritte's palette in both pictorial layers [157].

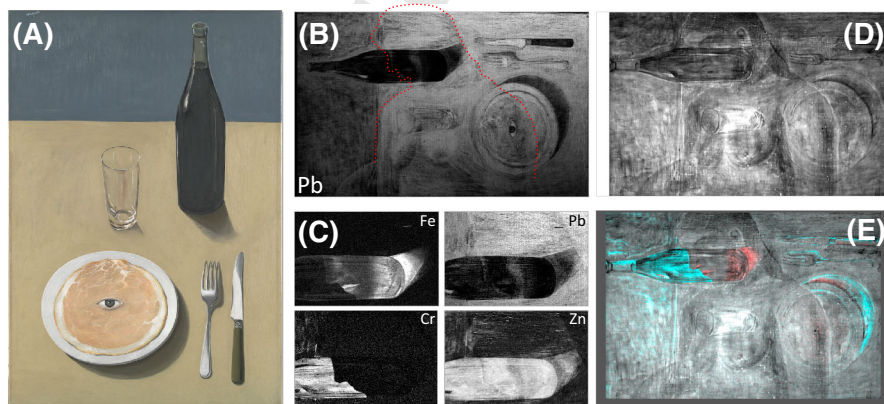


Fig. 10 **a** “Le portrait”, René Magritte (*The Portrait*, 1935; oil on canvas, 73.3_50.2 cm; Metropolitan Museum of Modern Art—(c) C. Herscovici/Artists Rights Society (ARS), New York, USA); **b** rotated MA-XRF Pb-L map; **c** different detailed MA-XRF of the facial area with adjusted contrast; **d** first transmission mode NIR eigenimage of 1000–1500 nm spectral region (after histogram equalization); **e** composite image obtained by overlaying the image of **d** with Cr (light blue), Fe + Hg (red) MA-XRF maps. Adapted from [157]

The results of these investigations are summarized in Fig. 10. The Pb distribution map (Fig. 10b) bears a significant and expected resemblance to the X-radiography, but is no longer encumbered by the stretcher and hardware and thus easier to interpret. The brushstrokes around the bottle confirm that the bottle was painted right on the top of original painting and that the background around it was painted afterwards. The female figure is visible in the Pb map, showing that this element is more abundant in the highlights of her face and body. The Zn distribution map, looking like the negative of the Pb map, suggests the presence of this element in the ground layer. The dark color used in the bottle appears to stem mainly from carbon black, as Ca and P appear co-localized; Magritte used this pigment also in other paintings. Next to K and Fe, also Cd is detected in the black. It is not unusual for Magritte to modify the tonality of his blacks by mixing with other colors, such as cadmium yellow, in his palette. The same elements are also present in the dark green used to paint the shadow of the plate, the haft of the knife and the top of the bottle. The relative proportions vary slightly as does the green tonality. No other element related to the inorganic green pigment could be identified, suggesting the green was produced by mixing bone black with cadmium yellow, painted over the blue sky of the hidden painting. In subsequent measurements diffuse reflectance spectroscopy (DRS) supports the use of a cadmium yellow in the dark glass of the bottle, its shadow and in the knife handle given the observation of a sharp transition edge at 470 nm, consistent with the presence of CdS [241]. The Cr XRF signals, recorded in the shadow of the plate and knife and in the top half part of the bottle, only, suggest that Magritte did not use a chromium oxide green pigment as part of the top-level blue nor in the dark paint of the bottle and shadows. Rather, this element is present in the sky of the underlying painting, its X-ray fluorescence likely to be totally blocked by the lead white in the top ochre paint while the top blue paint and especially the black and dark green paint are (partially) transparent for Cr XRF radiation. No metallic elements (such as Co, Cu, Fe) were detected that could relate to the blue color on the top half of the painting using the MA-XRF scanning. This rules out many blue pigments such as cobalt, Prussian or cerulean blue; however, ultramarine blue ($\text{Na}_{8-10}\text{Al}_6\text{Si}_6\text{O}_{24}\text{S}_{2-4}$) cannot be ruled out (Na, Al, Si, and S, characteristic elements of ultramarine, are all difficult or impossible to detect in typical MA-XRF experimental conditions). PXRF measurements using a He flush revealed weak peaks for Al and Si, supportive of the assignment of ultramarine. DRS measurements of the blue background revealed a broad absorption centered at 597 nm and a peak reflectance at 483 nm, also consistent with the presence of ultramarine blue. The green shifted reflectance maximum may in part be due to a contribution of the chrome oxide below. The red color of the slice of ham and of the eyelid were rendered with vermilion red; this pigment was also used in the underlying composition, in highlights over the nose and lips of the nude (Fig. 10c, e). The MA-XRF Fe and Pb maps as well as the diffuse reflectance measurements show that the rest of the figure was painted with an iron oxide based red pigment and lead white for the highlights. NIR hyperspectral imaging of the painting (400–2450 nm wavelength range) in transmission mode was found to give more information about the pictorial features of the prior painted composition than imaging in reflectance mode. Principle component analysis (PCA) analysis,



followed by histogram equalization was used to maximize the clarity of the features from the earlier painting [242, 243]. The appearance of the nude woman corresponds well to the photograph of the prior painting. In the spectral region from 1450 to 1680 nm, Minimum Noise Fraction PCA (MNF-PCA) yields a first eigenimage (Fig. 10d) that shows more of the sketches of the pictorial elements. Figure 10e clearly illustrates the complementary nature of MA-XRF and VNIR imaging. While in the darker areas, the XRF signals from the lower figure can more easily reach the XRF detector that is positioned in a reflection geometry, the opposite is true for the NIR signals that were recorded in transmission. The lighter, more lead white-rich paint is more transparent for the NIR photons while the dark, boneblack-rich areas efficiently absorb the NIR radiation. In this particular case, both imaging methods together are capable of revealing all details of the face, showing the characteristic enlarged lips, nose, ears and eyes that are expected.

5 Conclusions

In this review, an overview was presented of recent developments regarding the characterization of pigmented materials used by painters from the seventeenth to early twentieth century based on various forms of X-ray-based spectroscopic and imaging analysis. XRF covers a wide range of instrumentation that can be profitably employed for this type of investigations, ranging from fairly compact and cost-effective portable devices to sophisticated synchrotron beam lines where elemental imaging with submicroscopic lateral resolution is possible. Microscopic XRF is well suited to visualize the elemental distribution of key elements, mostly metals, present in paint multilayers on the length scale from 1 to 100 μm inside paint micro-samples taken from paintings. In the context of the characterization of the pigments that suffer from spontaneous degradation, the use of methods limited to elemental analysis or imaging usually is not sufficient to elucidate the chemical transformations that have taken place. However, at synchrotron facilities, combinations of $\mu\text{-XRF}$ with related methods such as $\mu\text{-XAS}$ and $\mu\text{-XRD}$ have proven themselves to be very suitable for such studies. Their use is often associated with $\mu\text{-FTIR}$ and $\mu\text{-RS}$ spectroscopy since these methods deliver complementary information on the molecular nature of the materials present, at more or less the same length scale as the X-ray microprobe techniques. The combined use of these methods has allowed elucidating the degradation pathways of some of the pigments frequently employed by fifteenth to twentieth century painters such as P.P. Rubens, Rembrandt van Rijn, V. van Gogh, J. Ensor, and H. Matisse. Some of these studies are now started to be combined with mapping of the distribution of pigments on the square metre scale.

References

1. Cotte M, Checroun E, De Nolf W, Taniguchi Y, De Viguier L, Burghammer M, Walter P, Rivard C, Salomé M, Janssens K, Susini J (2016) Lead soaps in paintings: friends or foes? *Stud Conserv*. doi:[10.1080/00393630.2016.1232529](https://doi.org/10.1080/00393630.2016.1232529)



2. Hendriks E (2011) Van Gogh's working practice: a technical study. In: Van Tilborgh L, Hendriks E (eds) Vincent Van Gogh Paintings 2: Antwerp & Paris, 1885–1888. Lund Humphries Publishers Ltd., London, pp 90–143
3. Jansen L, Luijten H, Bakker N (2009) Vincent van Gogh—The Letters. <http://www.vangoghletters.org>. Thames & Hudson Ltd., London
4. Janssens K, Alfeld M, Van der Snickt G, De Nolf W, Vanmeert F, Radepon M, Monico L, Dik J, Cotte M, Falkenberg G, Miliani C, Brunetti BG (2013) The use of synchrotron radiation for the characterization of artists' pigments and paintings. *Ann Rev Anal Chem* 6(6):399–425
5. Colombini MP, Modugno F (2004) Characterisation of proteinaceous binders in artistic paintings by chromatographic techniques. *J Sep Sci* 27:147–160
6. Vandenabeele P, Wehling B, Moens L, Dekeyser B, Cardon B, von Bohlen A, Klockenkamper R (1999) Pigment investigation of a late-medieval manuscript with total reflection X-ray fluorescence and micro-Raman spectroscopy. *Analyst* 124:169–172
7. Wess TJ, Drakopoulos M, Snigirev A, Wouters J, Paris O, Fratzl P, Collins M, Hiller J, Nielsen K (2001) The use of small-angle X-ray diffraction studies for the analysis of structural features in archaeological samples. *Archaeometry* 43:117–129
8. Cesaratto A, D'Andrea C, Nevin A, Valentini G, Tassone F, Alberti R, Frizzi T, Comelli D (2014) Analysis of cadmium-based pigments with time-resolved photoluminescence. *Anal Methods* 6:130–138
9. Antunes V, Jose Oliveira M, Vargas H, Serrao V, Candeias A, Carvalho ML, Coroado J, Mirao J, Dias L, Longelin S, Seruya AI (2014) Characterization of glue sizing under calcium carbonate ground layers in Flemish and Luso-Flemish painting—analysis by SEM-EDS, mu-XRD and mu-Raman spectroscopy. *Anal Methods* 6:710–717
10. Lluveras A, Boulerand S, Roque J, Cotte M, Giraldez P, Vendrell-Saz M (2008) Weathering of gilding decorations investigated by SR: development and distribution of calcium oxalates in the case of Sant Benet de Bages (Barcelona, Spain). *Appl Phys Mater Sci Process* 90:23–33
11. Bell IM, Clark RJH, Gibbs PJ (1997) Raman spectroscopic library of natural and synthetic pigments (pre-similar to 1850 AD). *Spectrochim Acta Part A Mol Biomol Spectrosc* 53:2159–2179
12. Van der Snickt G, De Nolf W, Vekemans B, Janssens K (2008) mu-XRF/mu-RS vs. SR mu-XRD for pigment identification in illuminated manuscripts. *Appl Phys A Mater Sci Process* 92:59–68
13. Andreotti A, Bonaduce I, Colombini MP, Gautier G, Modugno F, Ribechini E (2006) Combined GC/MS analytical procedure for the characterization of glycerolipid, waxy, resinous, and proteinaceous materials in a unique paint microsample. *Anal Chem* 78:4490–4500
14. Colombini MP, Andreotti A, Bonaduce I, Modugno F, Ribechini E (2010) Analytical strategies for characterizing organic paint media using gas chromatography/mass spectrometry. *Acc Chem Res* 43:715–727
15. Degano I, Ribechini E, Modugno F, Colombini MP (2009) Analytical methods for the characterization of organic dyes in artworks and in historical textiles. *Appl Spectrosc Rev* 44:363–410
16. Janssens K, Adams F, Rindby A (2000) Microscopic X-ray fluorescence analysis. Wiley, Chichester
17. Cotte M, Susini J, Dik J, Janssens K (2010) Synchrotron-based X-ray absorption spectroscopy for art conservation: looking back and looking forward. *Acc Chem Res* 43:705–714
18. De Nolf W, Janssens K (2010) Micro X-ray diffraction and fluorescence tomography for the study of multilayered automotive paints. *Surf Interface Anal* 42:411–418
19. Thoury M, Echard JP, Refregiers M, Berrie B, Nevin A, Jamme F, Bertrand L (2011) Synchrotron UV-visible multispectral luminescence microimaging of historical samples. *Anal Chem* 83:1737–1745
20. Bertrand L, Robinet L, Thoury M, Janssens K, Cohen SX, Schoder S (2012) Cultural heritage and archaeological materials studied by synchrotron spectroscopy and imaging. *Appl Phys A Mater Sci Process* 106:377–396
21. Janssens K, Legrand S, Van der Snickt G, Vanmeert F (2016) Virtual archaeology of altered paintings: multiscale chemical imaging tools. *Elements* 12:39–44
22. Janssens K, Dik J, Cotte M, Susini J (2010) Photon-based techniques for nondestructive subsurface analysis of painted cultural heritage artifacts. *Acc Chem Res* 43:814–825
23. Alfeld M, Broekaert JAC (2013) Mobile depth profiling and sub-surface imaging techniques for historical paintings—a review. *Spectrochim Acta Part B* 88:211–230
24. Miliani C, Rosi F, Brunetti BG, Sgamellotti A (2010) In situ noninvasive study of artworks: the MOLAB multitechnique approach. *Acc Chem Res* 43:728–738



25. Daffara C, Parisotto S, Mariotti PI (2015) Mid-infrared thermal imaging for an effective mapping of surface materials and sub-surface detachments in mural paintings: integration of thermography and thermal quasi-reflectography. In: Pezzati L, Targowski P (eds) Optics for arts, architecture, and archaeology V
26. Alfeld M, Janssens K, Dik J, de Nolf W, van der Snickt G (2011) Optimization of mobile scanning macro-XRF systems for the in situ investigation of historical paintings. *J Anal At Spectrom* 26:899–909
27. Dooley KA, Conover DM, Glinsman LD, Delaney JK (2014) Complementary standoff chemical imaging to map and identify artist materials in an early italian renaissance panel painting. *Angew Chem Int Edit* 53:13775–13779
28. De Nolf W, Dik J, Van der Snickt G, Wallert A, Janssens K (2011) High energy X-ray powder diffraction for the imaging of (hidden) paintings. *J Anal At Spectrom* 26:910–916
29. Legrand S, Alfeld M, Vanmeert F, De Nolf W, Janssens K (2014) Macroscopic Fourier transform infrared scanning in reflection mode (MA-rFTIR), a new tool for chemical imaging of cultural heritage artefacts in the mid-infrared range. *Analyst* 139:2489–2498
30. Daffara C, Pampaloni E, Pezzati L, Barucci M, Fontana R (2010) Scanning multispectral IR reflectography SMIRR: an advanced tool for art diagnostics. *Acc Chem Res* 43:847–856
31. Beckhoff B, Kanngiesser B, Langhoff N, Rainer W, Helmut W (2006) Handbook of practical X-ray fluorescence analysis. Springer, Berlin
32. Vincze L, Somogyi A, Osan J, Vekemans B, Torok S, Janssens K, Adams F (2002) Quantitative trace element analysis of individual fly ash particles by means of X-ray microfluorescence. *Anal Chem* 74:1128–1135
33. Vincze L, Janssens K, Adams F, Jones KW (1995) A general monte carlo simulation of energy-dispersive X-ray fluorescence spectrometers.3. Polarized polychromatic radiation, homogeneous samples. *Spectrochim Acta Part B At Spectrosc* 50:1481–1500
34. Vincze L, Janssens K, Vekemans B, Adams F (1999) Monte Carlo simulation of X-ray fluorescence spectra: part 4. Photon scattering at high X-ray energies. *Spectrochim Acta Part B At Spectrosc* 54:1711–1722
35. Lahanier C, Amsel G, Heitz C, Menu M, Andersen HH (1986) Proceedings of the international workshop on ion-beam analysis in the arts and archaeology—Pont-A-Mousson, Abbaye Des Pre-montres, France, February 18–20, 1985—Editorial. *Nucl Instrum Methods Phys Res Sect B Beam Interact Mater At* 14: R7–R8
36. Van Grieken R, Markowicz A (2002) Handbook of X-ray spectrometry. Marcel Dekker, New York
37. Van der Linden V, Meesdonk E, Devos A, Van Dooren R, Nieuwdorp H, Janssen E, Balace S, Vekemans B, Vincze L, Janssens K (2011) PXRF, mu-XRF, Vacuum mu-XRF, and EPMA Analysis of Email Champeve Objects Present in Belgian Museums. *Microsc Microanal* 17:674–685
38. Carvalho ML, Karydas A, Piorek S (2010) Special issue: the use and application of handheld and portable XRF spectrometers. *X-Ray Spectrom* 39:77
39. Potts PJ, Ramsey MH, Carlisle J (2002) Portable X-ray fluorescence in the characterisation of arsenic contamination associated with industrial buildings at a heritage arsenic works site near Redruth, Cornwall, UK. *J Environ Monit* 4:1017–1024
40. Jones MC, Williams-Thorpe O, Potts PJ, Webb PC (2005) Using field-portable XRF to assess geochemical variations within and between dolerite outcrops of Preseli, south Wales. *Geostand Geoanal Res* 29:251–269
41. Piorek S (1997) Field-portable X-ray fluorescence spectrometry: past, present, and future. *Field Anal Chem Technol* 1:317–329
42. Piorek S (2004) Ieee, Portable X-ray fluorescence analyzer for the first level screening of materials for prohibited substances, 2005 International Conference on Asian Green Electronics: Design for Manufacturability and Reliability, Proceedings, pp 7–13
43. Piorek S, Puusaari E, Piorek E, McCann B (1999) Identification and quantitative analysis of alloys using x-ray fluorescence analyzer with a silicon “p-i-n” diode detector. In: Fernandez JE, Tartari A (eds) EDXRS-98: Proceedings of the European Conference on Energy Dispersive X-Ray Spectrometry 1998. Editrice Compositori, Bologna, p 280
44. Pages-Camagna S, Laval E, Vigears D, Duran A (2010) Non-destructive and in situ analysis of Egyptian wall paintings by X-ray diffraction and X-ray fluorescence portable systems. *Appl Phys A Mater Sci Process* 100:671–681
45. Eveno M, Moignard B, Castaing J (2011) Portable apparatus for in situ X-ray diffraction and fluorescence analyses of artworks. *Microsc Microanal* 17:667–673



46. Kriznar A, Munoz V, de la Paz F, Respaldiza MA, Vega M (2011) Portable XRF study of pigments applied in Juan Hispalense's 15th century panel painting. *X-Ray Spectrom* 40:96–100
47. Migliori A, Bonanni P, Carraresi L, Grassi N, Mando PA (2011) A novel portable XRF spectrometer with range of detection extended to low-Z elements. *X-Ray Spectrom* 40:107–112
48. Kenna TC, Nitsche FO, Herron MM, Mailloux BJ, Petet D, Sritirairat S, Sands E, Baumgarten J (2011) Evaluation and calibration of a Field Portable X-Ray Fluorescence spectrometer for quantitative analysis of siliciclastic soils and sediments. *J Anal At Spectrom* 26:395–405
49. Tykot RH (2016) Using nondestructive portable X-ray fluorescence spectrometers on stone, ceramics, metals, and other materials in museums: advantages and limitations. *Appl Spectrosc* 70:42–56
50. Galli A, Bonizzoni L (2014) True versus forged in the cultural heritage materials: the role of PXRF analysis. *X-Ray Spectrom* 43:22–28
51. Beck L, Rousseliere H, Castaing J, Duran A, Lebon M, Moignard B, Plassard F (2014) First use of portable system coupling X-ray diffraction and X-ray fluorescence for in situ analysis of prehistoric rock art. *Talanta* 129:459–464
52. Pitarch A, Ruiz JF, de Vallejuelo SFO, Hernanz A, Maguregui M, Madariaga JM (2014) In situ characterization by Raman and X-ray fluorescence spectroscopy of post-Paleolithic blackish pictographs exposed to the open air in Los Chaparros shelter (Albalate del Arzobispo, Teruel, Spain). *Anal Methods* 6:6641–6650
53. Dayer L, d'Errico F, Garcia-Moreno R (2014) Searching for consistencies in Chatelperronian pigment use. *J Archaeol Sci* 44:180–193
54. Bracci S, Caruso O, Galeotti M, Iannaccone R, Magrini D, Picchi D, Pinna D, Porcinai S (2015) Multidisciplinary approach for the study of an Egyptian coffin (late 22nd/early 25th dynasty): combining imaging and spectroscopic techniques. *Spectrochim Acta Part A Mol Biomol Spectrosc* 145:511–522
55. Madariaga JM, Maguregui M, Castro K, Knuutinen U, Martinez-Arkarazo I (2016) Portable Raman, DRIFTS, and XRF analysis to diagnose the conservation state of two wall painting panels from pompeii deposited in the Naples National Archaeological Museum (Italy). *Appl Spectrosc* 70:137–146
56. Madariaga JM (2015) Analytical chemistry in the field of cultural heritage. *Anal Methods* 7:4848–4876
57. Crupi V, Galli G, La Russa MF, Longo F, Maisano G, Majolino D, Malagodi M, Pezzino A, Ricca M, Rossi B, Ruffolo SA, Venuti V (2015) Multi-technique investigation of Roman decorated plasters from Villa dei Quintili (Rome, Italy). *Appl Surf Sci* 349:924–930
58. Gomez-Moron MA, Ortiz P, Martin-Ramirez JM, Ortiz R, Castaing J (2016) A new insight into the vaults of the kings in the Alhambra (Granada, Spain) by combination of portable XRD and XRF. *Microchem J* 125:260–265
59. Syta O, Rozum K, Choinska M, Zielinska D, Zukowska GZ, Kijowska A, Wagner B (2014) Analytical procedure for characterization of medieval wall-paintings by X-ray fluorescence spectrometry, laser ablation inductively coupled plasma mass spectrometry and Raman spectroscopy. *Spectrochim Acta Part B At Spectrosc* 101:140–148
60. Daveri A, Doherty B, Moretti P, Grazia C, Romani A, Fiorini E, Brunetti BG, Vagnini M (2015) An uncovered XIII century icon: particular use of organic pigments and gilding techniques highlighted by analytical methods. *Spectrochim Acta Part A Mol Biomol Spectrosc* 135:398–404
61. Cechak T, Trojek T, Sefcu R, Chlumska S, Trestikova A, Kotrly M, Turkova I (2015) The use of powdered bismuth in Late Gothic painting and sculpture polychromy. *J Cult Herit* 16:747–752
62. Hradil D, Hradilova J, Bezdieka P, Svarcova S, Cermakova Z, Kosarova V, Nemec I (2014) Crocoite PbCrO₄ and mimetite Pb-5(AsO₄)(3)Cl: rare minerals in highly degraded mediaeval murals in Northern Bohemia. *J Raman Spectrosc* 45:848–858
63. Van der Snickt G, Miliani C, Janssens K, Brunetti BG, Romani A, Rosi F, Walter P, Castaing J, De Nolf W, Klaassen L, Labarque I, Wittermann R (2011) Material analyses of 'Christ with singing and music-making Angels', a late 15th-C panel painting attributed to Hans Memling and assistants: part I. non-invasive in situ investigations. *J Anal At Spectrom* 26:2216–2229
64. Duran A, Lopez-Montes A, Castaing J, Espejo T (2014) Analysis of a royal 15th century illuminated parchment using a portable XRF-XRD system and micro-invasive techniques. *J Archaeol Sci* 45:52–58
65. Van de Voorde L, Van Pevenage J, De Langhe K, De Wolf R, Vekemans B, Vincze L, Vandenberghe P, Martens MPJ (2014) Non-destructive in situ study of "Mad Meg" by Pieter Bruegel the



- Elder using mobile X-ray fluorescence, X-ray diffraction and Raman spectrometers. *Spectrochim Acta Part B At Spectrosc* 97:1–6
66. Veiga A, Teixeira DM, Candeias AJ, Mirao J, Manhita A, Miguel C, Rodrigues P, Teixeira JG (2015) Micro-analytical study of two seventeenth century gilded miniature portraits on copper. *Microchem J* 123:51–61
67. Roldan C, Juanes D, Ferrazza L, Carballo J (2016) Characterization of Sorolla's gouache pigments by means of spectroscopic techniques. *Radiat Phys Chem* 119:253–263
68. Van der Snickt G, Janssens K, Schalm O, Aibeo C, Kloust H, Alfeld M (2010) James Ensor's pigment use: artistic and material evolution studied by means of portable X-ray fluorescence spectrometry. *X-Ray Spectrom* 39:103–111
69. Kosarova V, Hradil D, Hradilova J, Cermakova Z, Nemec I, Schreiner M (2016) The efficiency of micro-Raman spectroscopy in the analysis of complicated mixtures in modern paints: munch's and Kupka's paintings under study. *Spectrochim Acta Part A Mol Biomol Spectrosc* 156:36–46
70. Kajiya EAM, Campos P, Rizzutto MA, Appoloni CR, Lopes F (2014) Evaluation of the veracity of one work by the artist Di Cavalcanti through non-destructive techniques: XRF, imaging and brush stroke analysis. *Radiat Phys Chem* 95:373–377
71. Cardeira AM, Longelin S, Costa S, Candeias A, Carvalho ML, Manso M (2014) Multi-analytical characterisation of D'Apres Cormon by Jose Veloso Salgado. *Nucl Instrum Methods Phys Res Sect B Beam Interact Mater At* 331:271–274
72. Izzo FC, Capogrosso V, Girona M, Alberti R, Mazzei C, Nodari L, Gambirasi A, Zendri E, Nevin A (2015) Multi-analytical non-invasive study of modern yellow paints from postwar Italian paintings from the International Gallery of Modern Art Ca Pesaro, Venice. *X-Ray Spectrom* 44:296–304
73. Trojek T, Trojkova D (2015) Several approaches to the investigation of paintings with the use of portable X-ray fluorescence analysis. *Radiat Phys Chem* 116:321–325
74. Cardeira AM, Longelin S, Costa S, Candeias A, Carvalho ML, Manso M (2016) Analytical characterization of academic nude paintings by Jose Veloso Salgado. *Spectrochim Acta Part A Mol Biomol Spectrosc* 153:379–385
75. Epley BA, Rogge CE (2015) Prior states: evolution of composition and color in two Barnett Newman paintings. *Appl Phys A Mater Sci Process* 121:987–998
76. Janssens K, Vekemans B, Vincze L, Adams F, Rindby A (1996) A micro-XRF spectrometer based on a rotating anode generator and capillary optics. *Spectrochim Acta Part B At Spectrosc* 51:1661–1678
77. Vincze L, Janssens K, Adams F, Rindby A, Engstrom P (1998) Interpretation of capillary generated spatial and angular distributions of x rays: theoretical modeling and experimental verification using the European Synchrotron Radiation Facility Optical beam line. *Rev Sci Instrum* 69:3494–3503
78. Schroer CG, Boye P, Feldkamp JM, Patommel J, Samberg D, Schropp A, Schwab A, Stephan S, Falkenberg G, Wellenreuther G, Reimers N (2010) Hard X-ray nanoprobe at beamline P06 at PETRA III. *Nucl Instrum Methods Phys Res Sect A Accel Spectrom Detect Assoc Equip* 616:93–97
79. Lengeler B, Schroer CG, Benner B, Gerhardus A, Gunzler TF, Kuhlmann M, Meyer J, Zimprich C (2002) Parabolic refractive X-ray lenses. *J Synchrotron Radiat* 9:119–124
80. Gorelick S, Vila-Comamala J, Guzenko VA, Barrett R, Salome M, David C (2011) High-Efficiency Gold Fresnel Zone Plates for Multi-keV X-rays. In: McNulty I, Eyberger C, Lai B (eds) 10th International Conference on X-Ray Microscopy, pp 88–91
81. Sarkar SS, Sahoo PK, Solak HH, David C, Van der Veen JF (2008) Fabrication of Fresnel zone plates by holography in the extreme ultraviolet region. *J Vac Sci Technol B* 26:2160–2163
82. Alianelli L, Sawhney KJS, Barrett R, Pape I, Malik A, Wilson MC (2011) High efficiency nano-focusing kinoform optics for synchrotron radiation. *Opt Express* 19:11120–11127
83. Barrett R, Baker R, Cloetens P, Dabin Y, Morawe C, Suhonen H, Tucoulou R, Vivo A, Zhang L (2011) Dynamically-figured mirror system for high-energy nanofocusing at the ESRF, Conference on Advances in X-Ray/EUV Optics and Components VISan Diego, CA
84. Bichlmeier S, Janssens K, Heckel J, Gibson D, Hoffmann P, Ortner HM (2001) Component selection for a compact micro-XRF spectrometer. *X-Ray Spectrom* 30:8–14
85. Trentelman K, Bouchard M, Ganio M, Namowicz C, Patterson CS, Walton M (2010) The examination of works of art using in situ XRF line and area scans. *X-Ray Spectrom* 39:159–166
86. Buzanich G, Wobraschek P, Strelci A, Markowicz A, Wegrzynek D, Chineano E, Griesser M, Uhlir K (2010) PART II (Portable ART analyzer)—development of a XRF spectrometer adapted for the study of artworks in the Kunsthistorisches Museum, Vienna. *X-Ray Spectrom* 39:98–102



87. Vittiglio G, Bichhneier S, Klinger P, Heckel J, Fuzhong W, Vincze L, Janssens K, Engstrom P, Rindby A, Dietrich K, Jembrih-Simburger D, Schreiner M, Denis D, Lakdar A, Lamotte A (2004) A compact mu-XRF spectrometer for (in situ) analyses of cultural heritage and forensic materials. *Nucl Instrum Methods Phys Res Sect B Beam Interact Mater At* 213:693–698
88. Bronk H, Rohrs S, Bjeoumikhov A, Langhoff N, Schmalz J, Wedell R, Gorny HE, Herold A, Waldschlager U (2001) ArtTAX—a new mobile spectrometer for energy-dispersive micro X-ray fluorescence spectrometry on art and archaeological objects. *Fresenius J Anal Chem* 371:307–316
89. Rabin I, Hahn O (2013) Characterization of the Dead Sea Scrolls by advanced analytical techniques. *Anal Methods* 5:4648–4654
90. Wolff T, Rabin I, Mantouvalou I, Kanngiesser B, Malzer W, Kindzorra E, Hahn O (2012) Provenance studies on Dead sea scrolls parchment by means of quantitative micro-XRF. *Anal Bioanal Chem* 402:1493–1503
91. Valerio P, Silva RJC, Araujo MF, Soares AMM, Barros L (2012) A multianalytical approach to study the Phoenician bronze technology in the Iberian Peninsula-A view from Quinta do Almaraz. *Mater Charact* 67:74–82
92. Figueiredo E, Araujo MF, Silva RJC, Senna-Martinez JC, Vaz JLI (2011) Characterisation of Late Bronze Age large size shield nails by EDXRF, micro-EDXRF and X-ray digital radiography. *Appl Radiat Isot* 69:1205–1211
93. Herm C (2008) Mobile micro-X-ray fluorescence analysis (XRF) on medieval paintings. *Chimia* 62:887–898
94. Cheng L, Li MT, Youshi K, Fan CS, Wang SH, Pan QL, Liu ZG, Li RW (2011) The study of chemical composition and elemental mappings of colored over-glaze porcelain fired in Qing Dynasty by micro-X-ray fluorescence. *Nucl Instrum Methods Phys Res Sect B Beam Interact Mater At* 269:239–243
95. Dietz G, Ketelsen T, Hoss M, Simon O, Wintermann C, Wolff T, Rabin I, Hahn O (2012) The Egmont Master phenomenon: X-ray fluorescence spectrometric and paper studies for art history research. *Anal Bioanal Chem* 402:1505–1515
96. Sun TX, Ding XL (2015) Confocal X-ray technology based on capillary X-ray optics. *Rev Anal Chem* 34:45–59
97. Janssens K, Proost K, Falkenberg G (2004) Confocal microscopic X-ray fluorescence at the HASYLAB microfocus beamline: characteristics and possibilities. *Spectrochim Acta Part B At Spectrosc* 59:1637–1645
98. Woll AR, Agyeman-Budu D, Choudhury S, Coulthard I, Finnefrock AC, Gordon R, Hallin E, Mass J (2014) Lithographically-fabricated channel arrays for confocal X-ray fluorescence microscopy and XAFS. In: Arp U, Reversz P, Williams GP (eds) 17th Pan-American Synchrotron Radiation Instrumentation Conference Sri2013
99. Bjeoumikhov A, Erko M, Bjeoumikhova S, Erko A, Snigireva I, Snigirev A, Wolff T, Mantouvalou I, Malzer W, Kanngiesser B (2008) Capillary mu Focus X-ray lenses with parabolic and elliptic profile. *Nucl Instrum Methods Phys Res Sect A Accel Spectrom Detect Assoc Equip* 587:458–463
100. Luhl L, Mantouvalou I, Schaumann I, Vogt C, Kanngiesser B (2013) Three-dimensional chemical mapping with a confocal xrf setup. *Anal Chem* 85:3682–3689
101. Woll AR, Agyeman-Budu D, Bilderback DH, Dale D, Kazimirov AY, Pfeifer M, Plautz T, Szebenyi T, Untracht G (2012) 3D X-ray fluorescence microscopy with 1.7 μm resolution using lithographically fabricated micro-channel arrays. In: Goto S, Morawe C, Khounsary AM (eds.) *Advances in X-Ray/Euv Optics and Components VII*
102. Beckhoff B, Fliegauf R, Ulm G, Weser J, Pepponi G, Strelci C, Wobrauschek P, Ehmann T, Fabry L, Mantler C, Pahlke S, Kanngiesser B, Malzer W (2003) Ultra-trace analysis of light elements and speciation of minute organic contaminants on silicon wafer surfaces by means of TXRF in combination with NEXAFS. *International Society for Optical Engineering*, pp 120–128
103. Woll AR, Bilderback DH, Gruner S, Gao N, Huang R, Bisulca C, Mass J (2005) Confocal x-ray fluorescence (XRF) microscopy: a new technique for the nondestructive compositional depth profiling of paintings. In: Vandiver PB, Mass JL, Murray A (eds) *Materials issues in art and archaeology VII*
104. Woll AR, Mass J, Bisulca C, Huang R, Bilderback DH, Gruner S, Gao N (2006) Development of confocal X-ray fluorescence (XRF) microscopy at the Cornell high energy synchrotron source. *Appl Phys A Mater Sci Process* 83
105. Smit Z, Janssens K, Proost K, Langus I (2004) Confocal mu-XRF depth analysis of paint layers. *Nucl Instrum Methods Phys Res Sect B Beam Interact Mater At* 219:35–40



106. Tsuji K, Matsuno T, Takimoto Y, Yamanashi M, Kometani N, Sasaki YC, Hasegawa T, Kato S, Yamada T, Shoji T, Kawahara N (2015) New developments of X-ray fluorescence imaging techniques in laboratory. *Spectrochim Acta Part B At Spectrosc* 113:43–53
107. Polese C, Cappuccio G, Dabagov SB, Hampai D, Liedl A, Pace E (2015) 2D and 3D micro-XRF based on polycapillary optics at XLab Frascati. In: Goto S, Morawe C, Khounsary AM (eds) *Advances in X-Ray/Euv Optics and Components X*
108. Smolek S, Nakazawa T, Tabe A, Nakano K, Tsuji K, Strelci C, Wobrauschek P (2014) Comparison of two confocal micro-XRF spectrometers with different design aspects. *X-Ray Spectrom* 43:93–101
109. Nakazawa T, Tsuji K (2013) Development of a high-resolution confocal micro-XRF instrument equipped with a vacuum chamber. *X-Ray Spectrom* 42:374–379
110. Mantouvalou I, Lange K, Wolff T, Grotzsch D, Luhl L, Haschke M, Hahn O, Kanngiesser B (2010) A compact 3D micro X-ray fluorescence spectrometer with X-ray tube excitation for archaeometric applications. *J Anal At Spectrom* 25:554–561
111. Tsuji K, Tabe A, Wobrauschek P, Strelci C (2015) Secondary excitation process for quantitative confocal 3D-XRF analysis. *Powder Diffr* 30:109–112
112. Wrobel P, Wegrzynek D, Czyzycki M, Lankosz M (2014) Depth profiling of element concentrations in stratified materials by confocal microbeam X-ray fluorescence spectrometry with polychromatic excitation. *Anal Chem* 86:11275–11280
113. Mantouvalou I, Wolff T, Seim C, Stoytschew V, Malzer W, Kanngiesser B (2014) Reconstruction of confocal micro-X-ray fluorescence spectroscopy depth scans obtained with a laboratory setup. *Anal Chem* 86:9774–9780
114. Czyzycki M, Wrobel P, Lankosz M (2014) Confocal X-ray fluorescence micro-spectroscopy experiment in tilted geometry. *Spectrochim Acta Part B At Spectrosc* 97:99–104
115. Huber C, Smolek S, Strelci C (2014) Simulation of layer measurement with confocal micro-XRF. *X-Ray Spectrom* 43:175–179
116. Wrobel P, Czyzycki M (2013) Direct deconvolution approach for depth profiling of element concentrations in multi-layered materials by confocal micro-beam X-ray fluorescence spectrometry. *Talanta* 113:62–67
117. Mantouvalou I, Malzer W, Kanngiesser B (2012) Quantification for 3D micro X-ray fluorescence. *Spectrochim Acta Part B At Spectrosc* 77:9–18
118. Schoonjans T, Silversmit G, Vekemans B, Schmitz S, Burghammer M, Riekel C, Brenker FE, Vincze L (2012) Fundamental parameter based quantification algorithm for confocal nano-X-ray fluorescence analysis. *Spectrochim Acta Part B At Spectrosc* 67:32–42
119. Laclavetine K, Ager FJ, Arquillo J, Respaldiza MA, Scrivano S (2016) Characterization of the new mobile confocal micro X-ray fluorescence (CXRF) system for in situ non-destructive cultural heritage analysis at the CNA: mu XRF-CONCHA. *Microchem J* 125:62–68
120. Reiche I, Muller K, Mysak E, Eveno M, Mottin B (2015) Toward a three-dimensional vision of the different compositions and the stratigraphy of the painting L'Homme bless, by G. Courbet: coupling SEM-EDX and confocal micro-XRF. *Appl Phys A Mater Sci Process* 121:903–913
121. Sun TX, Liu ZG, Wang GF, Ma YZ, Peng S, Sun WY, Li FZ, Sun XP, Ding XL (2014) Application of confocal X-ray fluorescence micro-spectroscopy to the investigation of paint layers. *Appl Radiat Isot* 94:109–112
122. Woll AR, Mass J, Bisulca C, Cushi-Nan M, Griggs C, Wanzy T, Ocon N (2008) The Unique History of The Armorer's Shop an application of confocal x-ray fluorescence microscopy. *Stud Conserv* 53:93–109
123. Kanngiesser B, Malzer W, Mantouvalou I, Sokaras D, Karydas AG (2012) A deep view in cultural heritage-confocal micro X-ray spectroscopy for depth resolved elemental analysis. *Appl Phys A Mater Sci Process* 106:325–338
124. Reiche I, Mueller K, Eveno M, Itie E, Menu M (2012) Depth profiling reveals multiple paint layers of Louvre Renaissance paintings using non-invasive compact confocal micro-X-ray fluorescence. *J Anal At Spectrom* 27:1715–1724
125. Yi LT, Liu ZG, Wang K, Lin X, Chen M, Peng SQ, Yang K, Wang JB (2016) Combining depth analysis with surface morphology analysis to analyse the prehistoric painted pottery from Majiayao Culture by confocal 3D-XRF. *Appl Phys A Mater Sci Process* 122
126. Choudhury S, Hormes J, Agyeman-Budu DN, Woll AR, George GN, Coulthard I, Pickering IJ (2015) Application of a spoked channel array to confocal X-ray fluorescence imaging and X-ray absorption spectroscopy of medieval stained glass. *J Anal At Spectrom* 30:759–766



127. Kanngiesser B, Mantouvalou I, Malzer W, Wolff T, Hahn O (2008) Non-destructive, depth resolved investigation of corrosion layers of historical glass objects by 3D Micro X-ray fluorescence analysis. *J Anal At Spectrom* 23:814–819
128. Yagi R, Tsuji K (2015) Confocal micro-XRF analysis of light elements with Rh X-ray tube and its application for painted steel sheet. *X-Ray Spectrom* 44:186–189
129. Li FZ, Liu ZG, Sun TX, Yi LT, Zhao WG, He JL, Peng S, Wang LL, Zhao GC, Ding XL (2015) Application of three dimensional confocal micro X-Ray fluorescence technology based on polycapillary X-Ray lens in analysis of rock and mineral samples. *Spectrosc Spectr Anal* 35:2487–2491
130. Janssens K, Vittiglio G, Deraedt I, Aerts A, Vekemans B, Vincze L, Wei F, Deryck I, Schalm O, Adams F, Rindby A, Knochel A, Simionovici A, Snigirev A (2000) Use of microscopic XRF for non-destructive analysis in art and archaeometry. *X-Ray Spectrom* 29:73–91
131. Terzano R, Spagnuolo M, Vekemans B, De Nolf W, Janssens K, Falkenberg G, Flore S, Ruggiero P (2007) Assessing the origin and fate of Cr, Ni, Cu, Zn, Pb, and V in industrial polluted soil by combined microspectroscopic techniques and bulk extraction methods. *Environ Sci Technol* 41:6762–6769
132. Janssens K, De Nolf W, Van Der Snickt G, Vincze L, Vekemans B, Terzano R, Brenker F (2010) Recent trends in quantitative aspects of microscopic X-ray fluorescence analysis. *Trac Trends Anal Chem* 29:464–478
133. Fittschen UEA, Falkenberg G (2011) Trends in environmental science using microscopic X-ray fluorescence. *Spectrochim Acta Part B At Spectrosc* 66:567–580
134. Salome M, Bleuet P, Bohic S, Cauzid J, Chalmin E, Cloetens P, Cotte M, De Andrade V, Martinez-Criado G, Petitgirard S, Rak M, Tresserras JAS, Szlachetko J, Tucoulou R, Susini J (2009) Fluorescence X-ray micro-spectroscopy activities at ESRF. In: David C, Nolting F, Quitmann C, Stampanoni M, Pfeiffer F (eds) 9th International Conference on X-Ray Microscopy Zurich, Switzerland, pp 012014
135. Hahn O, Oltrogge D, Bevers H (2004) Coloured prints of the 16th century: non-destructive analyses on coloured engravings from Albrecht Durer and contemporary artists. *Archaeometry* 46:273–282
136. Paternoster G, Rinziivillo R, Nunziata F, Castellucci EM, Lofrumento C, Zoppi A, Felici AC, Fronterotta G, Nicolais C, Piacentini M, Sciuti S, Vendittelli M (2005) Study on the technique of the Roman age mural paintings by micro-XRF with Polycapillary Conic Collimator and micro-Raman analyses. *J Cult Herit* 6:21–28
137. Bertrand L, Cotte M, Stampanoni M, Thoury M, Marone F, Schoeder S (2012) Development and trends in synchrotron studies of ancient and historical materials. *Phys Rep Rev Sect Phys Lett* 519:51–96
138. Gervais C, Thoury M, Reguer S, Gueriau P, Mass J (2015) Radiation damages during synchrotron X-ray micro-analyses of Prussian blue and zinc white historic paintings: detection, mitigation and integration. *Appl Phys A Mater Sci Process* 121:949–955
139. Bertrand L, Schoeder S, Anglos D, Breese MBH, Janssens K, Moini M, Simon A (2015) Mitigation strategies for radiation damage in the analysis of ancient materials. *Trac Trends Anal Chem* 66:128–145
140. Nuyts G, Cagno S, Bugani S, Janssens K (2015) Micro-XANES study on Mn browning: use of quantitative valence state maps. *J Anal At Spectrom* 30:642–650
141. Rietveld HM (1969) A profile refinement method for nuclear and magnetic structures. *J Appl Crystallogr* 2:65–71
142. Dik J, Janssens K, Van der Snickt G, van der Loeff L, Rickers K, Cotte M (2008) Visualization of a lost painting by Vincent van Gogh using synchrotron radiation based X-ray fluorescence elemental mapping. *Anal Chem* 80:6436–6442
143. Alfeld M, Janssens K (2015) Strategies for processing mega-pixel X-ray fluorescence hyperspectral data: a case study on a version of Caravaggio's painting Supper at Emmaus. *J Anal At Spectrom* 30:777–789
144. Dik J, Wallert A, Van der Snickt G, Janssens K (2008) Silverpoint underdrawing? A note on its visualization with synchrotron radiation based x-ray fluorescence analysis. *Zeitschrift für Kunsttechnologie und Konservierung* 22:381–384
145. Struick van der Loeff L, Alfeld M, Meedendorp T, Dik J, Hendriks E, van der Snickt G, Koen J, Meta C (2012) Rehabilitation of a flower still life in the Kröller-Müller Museum and a lost Antwerp painting by Van Gogh. In: van Tilborgh L (ed) Van Gogh: new findings. Van Gogh Museum, Amsterdam



- 1897
1898
1899
1900
1901
1902
1903
1904
1905
1906
1907
1908
1909
1910
1911
1912
1913
1914
1915
1916
1917
1918
1919
1920
1921
1922
1923
1924
1925
1926
1927
1928
1929
1930
1931
1932
1933
1934
1935
1936
1937
1938
1939
1940
1941
1942
1943
1944
1945
1946
1947
1948
1949
1950
1951
1952
146. Alfeld M, Janssens K, Appel K, Thijsse B, Blaas J, Dik J (2011) A portrait by Philipp Otto Runge—visualizing modifications to the painting using synchrotron-based X-ray fluorescence elemental scanning. *Zeitschrift für Kunsttechnologie und Konservierung* 25:157–163
147. Howard DL, de Jonge MD, Lau D, Hay D, Varcoe-Cocks M, Ryan CG, Kirkham R, Moorhead G, Paterson D, Thurrowgood D (2012) High-Definition X-ray fluorescence elemental mapping of paintings. *Anal Chem* 84:3278–3286
148. Alfeld M, Siddons DP, Janssens K, Dik J, Woll A, Kirkham R, van de Wetering E (2013) Visualizing the 17th century underpainting in Portrait of an Old Man by Rembrandt van Rijn using synchrotron-based scanning macro-XRF. *Appl Phys A Mater Sci Process* 111:157–164
149. Alfeld M, Pedroso JV, Hommes MVE, Van der Snickt G, Tauber G, Blaas J, Haschke M, Erler K, Dik J, Janssens K (2013) A mobile instrument for in situ scanning macro-XRF investigation of historical paintings. *J Anal At Spectrom* 28:760–767
150. Alfeld M, De Nolf W, Cagno S, Appel K, Siddons DP, Kuczewski A, Janssens K, Dik J, Trentelman K, Walton M, Sartorius A (2013) Revealing hidden paint layers in oil paintings by means of scanning macro-XRF: a mock-up study based on Rembrandt's "An old man in military costume". *J Anal At Spectrom* 28:40–51
151. Trentelman K, Janssens K, van der Snickt G, Szafran Y, Woollett AT, Dik J (2015) Rembrandt's An Old Man in Military Costume: the underlying image re-examined. *Appl Phys A Mater Sci Process* 121:801–811
152. Janssens K, Van der Snickt G, Alfeld M, Noble P, van Loon A, Delaney J, Conover D, Zeibel J, Dik J (2016) Rembrandt's 'Saul and David' (c. 1652): use of multiple types of smalt evidenced by means of non-destructive imaging. *Microchem J* 126:515–523
153. Noble P, van Loon A, Alfeld M, Janssens K, Dik J (2012) Rembrandt and/or Studio, Saul and David, c. 1655: visualising the curtain using cross-section analyses and X-ray fluorescence imaging. *Techné* 36:35–45
154. Verslype I (2012) The restoration of Woman in Blue Reading a Letter by Johannes Vermeer. *Rijksmuseum Bull* 60:2–19
155. Bull D, Krekeler A, Alfeld M, Dik J, Janssens K (2011) An intrusive portrait by Goya. *Burling Mag* 153:668–673
156. Monico L, Janssens K, Hendriks E, Vanmeert F, Van der Snickt G, Cotte M, Falkenberg G, Brunetti BG, Miliani C (2015) Evidence for degradation of the chrome yellows in van gogh's sunflowers: a study using noninvasive in situ methods and synchrotron-radiation-based X-ray techniques. *Angew Chem Int Edit* 54:13923–13927
157. Van der Snickt G, Martins A, Delaney J, Janssens K, Zeibel J, Duffy M, McGlinchey C, Van Driel B, Dik J (2016) Exploring a hidden painting below the surface of Rene Magritte's Le Portrait. *Appl Spectrosc* 70:57–67
158. Martins A, Albertson C, McGlinchey C, Dik J (2016) Piet Mondrian's Broadway Boogie Woogie: non invasive analysis using macro X-ray fluorescence mapping (MA-XRF) and multivariate curve resolution-alternating least square (MCR-ALS). *Herit Sci* 4:22. doi:10.1186/s40494-016-0091-4
159. Martins AMT, Coddington J, Snickt GVD, Driel BV, McGlinchey C, Dahlberg D, Janssens K, Dik J (2016) Jackson Pollock's Number 1A, 1948: A non-invasive study using Macro-X-Ray Fluorescence mapping (MA-XRF) and Multivariate Curve Resolution—Alternating Least Squares (MCR-ALS) analysis. *Herit Sci* 4 (in press)
160. Ravaut E, Pichon L, Laval E, Gonzalez V, Eveno M, Calligaro T (2016) Development of a versatile XRF scanner for the elemental imaging of paintworks. *Appl Phys A Mater Sci Process* 122
161. Anaf W, Schalm O, Janssens K, De Wael K (2015) Understanding the (in)stability of semiconductor pigments by a thermodynamic approach. *Dyes Pigm* 113:409–415
162. Da Pieve F, Stankowski M, Hogan C (2014) Electronic structure calculations of mercury mobilization from mineral phases and photocatalytic removal from water and the atmosphere. *Sci Total Environ* 493:596–605
163. Vanmeert F, Van der Snickt G, Janssens K (2015) Plumbonacrite identified by X-ray powder diffraction tomography as a missing link during degradation of red lead in a Van Gogh painting. *Angew Chem Int Edit* 54:3607–3610
164. Anaf W, Trashin S, Schalm O, van Dorp D, Janssens K, De Wael K (2014) Electrochemical photodegradation study of semiconductor pigments: influence of environmental parameters. *Anal Chem* 86:9742–9748



165. Hogan C, Da Pieve F (2015) Colour degradation of artworks: an ab initio approach to X-ray, electronic and optical spectroscopy analyses of vermilion photodarkening. *J Anal At Spectrom* 30:588–598
166. Emslie SD, Brasso R, Patterson WP, Valera AC, McKenzie A, Silva AM, Gleason JD, Blum JD (2015) Chronic mercury exposure in Late Neolithic/Chalcolithic populations in Portugal from the cultural use of cinnabar. *Sci Rep* 5
167. Radepont M, de Nolf W, Janssens K, Van der Snickt G, Coquinot Y, Klaassen L, Cotte M (2011) The use of microscopic X-ray diffraction for the study of HgS and its degradation products corderoite (α -Hg₃S₂Cl₂), kenhsuite (γ -Hg₃S₂Cl₂) and calomel (Hg₂Cl₂) in historical paintings. *J Anal At Spectrom* 26:959–968
168. Cotte M, Susini J, Metrich N, Moscato A, Gratzia C, Bertagnini A, Pagano M (2006) Blackening of Pompeian cinnabar paintings: X-ray microspectroscopy analysis. *Anal Chem* 78:7484–7492
169. Cotte M, Susini J, Sole VA, Taniguchi Y, Chillida J, Checroun E, Walter P (2008) Applications of synchrotron-based micro-imaging techniques to the chemical analysis of ancient paintings. *J Anal At Spectrom* 23:820–828
170. Radepont M, Coquinot Y, Janssens K, Ezrati J-J, de Nolf W, Cotte M (2015) Thermodynamic and experimental study of the degradation of the red pigment mercury sulfide. *J Anal At Spectrom* 30:599–612
171. Keune K, Boon JJ (2005) Analytical imaging studies clarifying the process of the darkening of vermilion in paintings. *Anal Chem* 77:4742–4750
172. Da Pieve F, Hogan C, Lamoën D, Verbeeck J, Vanmeert F, Radepont M, Cotte M, Janssens K, Gonze X, Van Tendeloo G (2013) Casting light on the darkening of colors in historical paintings. *Phys Rev Lett* 111
173. Anaf W, Janssens K, De Wael K (2013) Formation of Metallic Mercury During Photodegradation/ Photodarkening of α -HgS: electrochemical Evidence. *Angew Chem Int Ed* 52:12568–12571
174. Neiman MK, Balonis M, Kakoulli I (2015) Cinnabar alteration in archaeological wall paintings: an experimental and theoretical approach. *Appl Phys A Mater Sci Process* 121:915–938
175. Uda M (2004) In situ characterization of ancient plaster and pigments on tomb walls in Egypt using energy dispersive X-ray diffraction and fluorescence. *Nucl Instrum Methods Phys Res Sect B Beam Interact Mater At* 226:75–82
176. Daniels V, Leach B (2004) The occurrence and alteration of realgar on ancient Egyptian papyri. *Stud Conserv* 49:73–84
177. Muralha VSF, Burgio L, Clark RJH (2012) Raman spectroscopy analysis of pigments on 16–17th c. Persian manuscripts. *Spectrochim Acta Part A Mol Biomol Spectrosc* 92:21–28
178. Deneckere A, De Reu M, Martens MPJ, De Coene K, Vekemans B, Vincze L, De Maeyer P, Vandenabeele P, Moens L (2011) The use of a multi-method approach to identify the pigments in the 12th century manuscript *Liber Floridus*. *Spectrochim Acta Part A Mol Biomol Spectrosc* 80:125–132
179. Brown KL, Clark RJH (2004) The Lindisfarne Gospels and two other 8th century Anglo-Saxon/ Insular manuscripts: pigment identification by Raman microscopy. *J Raman Spectrosc* 35:4–12
180. Keune K, Mass J, Meirer F, Pottasch C, van Loon A, Hull A, Church J, Pouyet E, Cotte M, Mehta A (2015) Tracking the transformation and transport of arsenic sulfide pigments in paints: synchrotron-based X-ray micro-analyses. *J Anal At Spectrom* 30:813–827
181. Vermeulen M, Sanyova J, Janssens K (2015) Identification of artificial orpiment in the interior decorations of the Japanese tower in Laeken, Brussels, Belgium. *Herit Sci* 3:9
182. Trentelman K, Stodulski L, Pavlosky M (1996) Characterization of pararealgar and other light-induced transformation products from realgar by Raman microspectroscopy. *Anal Chem* 68:1755–1761
183. MunizMiranda M, Sbrana G, Bonazzi P, Menchetti S, Pratesi G (1996) Spectroscopic investigation and normal mode analysis of As₄S₄ polymorphs. *Spectrochim Acta Part A Mol Biomol Spectrosc* 52:1391–1401
184. Bindi L, Bonazzi P (2007) Light-induced alteration of arsenic sulfides: a new product with an orthorhombic crystal structure. *Am Miner* 92:617–620
185. Kyono A, Kimata M, Hatta T (2005) Light-induced degradation dynamics in realgar: in situ structural investigation using single-crystal X-ray diffraction study and X-ray photoelectron spectroscopy. *Am Miner* 90:1563–1570



186. Macchia A, Cesaro SN, Campanella L, Maras A, Rocchia M, Roscioli G (2013) Which light for cultural heritage: comparison of light sources with respect to realgar photodegradation. *J Appl Spectrosc* 80:637–643
187. Vermeulen M, Nuyts G, Sanyova J, Vila A, Buti D, Suuronen JP, Janssens K (2016) Visualization of As(III) and As(V) distributions in degraded paint micro-samples from Baroque- and Rococo-era paintings. *J Anal At Spectrom* 31:1913–1921
188. Boon JJ, Keune K, van der Weerd J, Geldof M, de Boer J (2001) Imaging microspectroscopic, secondary ion mass spectrometric and electron microscopic studies on discoloured and partially discoloured smalt in cross-sections of 16th century paintings. *Chimia* 55:952–960
189. Panighello S, Kavcic A, Vogel-Mikus K, Tennent NH, Wallert A, Hocevar SB, van Elteren JT (2016) Investigation of smalt in cross-sections of 17th century paintings using elemental mapping by laser ablation ICP-MS. *Microchem J* 125:105–115
190. Spring M, Higgitt C, Saunders D (2005) Investigation of Pigment-Medium Interaction Processes in Oil Paint containing Degraded Smalt. *Natl Gallery Tech Bull* 26:56–70
191. Robinet L, Spring M, Pages-Camagna S, Vantelon D, Trcera N (2011) Investigation of the discoloration of smalt pigment in historic paintings by micro-X-ray absorption spectroscopy at the Co K-Edge. *Anal Chem* 83:5145–5152
192. Robinet L, Spring M, Pages-Camagna S (2013) Vibrational spectroscopy correlated with elemental analysis for the investigation of smalt pigment and its alteration in paintings. *Anal Methods* 5:4628–4638
193. Cianchetta I, Colantoni I, Talarico F, d'Acapito F, Trapananti A, Maurizio C, Fantacci S, Davoli I (2012) Discoloration of the smalt pigment: experimental studies and ab initio calculations. *J Anal At Spectrom* 27:1941–1948
194. Miliani C, Daveri A, Brunetti BG, Sgamellotti A (2008) CO(2) entrapment in natural ultramarine blue. *Chem Phys Lett* 466:141–148
195. Gambardella AA, Patterson CMS, Webb SM, Walton MS (2016) Sulfur K-edge XANES of lazurite: toward determining the provenance of lapis lazuli. *Microchem J* 125:299–307
196. Salvado N, Buti S, Aranda MAG, Pradell T (2014) New insights on blue pigments used in 15th century paintings by synchrotron radiation-based micro-FTIR and XRD. *Anal Methods* 6:3610–3621
197. Pintus V, Wei SY, Schreiner M (2016) Accelerated UV ageing studies of acrylic, alkyd, and polyvinyl acetate paints: influence of inorganic pigments. *Microchem J* 124:949–961
198. Del Federico E, Shofberger W, Schelvis J, Kapetanaki S, Tyne L, Jerschow A (2006) Insight into framework destruction in ultramarine pigments. *Inorg Chem* 45:1270–1276
199. Cato E, Borca C, Huthwelker T, Ferreira ESB (2016) Aluminium X-ray absorption near-edge spectroscopy analysis of discoloured ultramarine blue in 20th century oil paintings. *Microchem J* 126:18–24
200. Monico L, Van der Snickt G, Janssens K, De Nolf W, Miliani C, Verbeeck J, Tian H, Tan H, Dik J, Radepon M, Cotte M (2011) Degradation process of lead chromate in paintings by Vincent van Gogh studied by means of synchrotron X-ray spectromicroscopy and related methods. 1. Artificially aged model samples. *Anal Chem* 83:1214–1223
201. Monico L, Van der Snickt G, Janssens K, De Nolf W, Miliani C, Dik J, Radepon M, Hendriks E, Geldof M, Cotte M (2011) Degradation process of lead chromate in paintings by Vincent van Gogh studied by means of synchrotron X-ray spectromicroscopy and related methods. 2. Original paint layer samples. *Anal Chem* 83:1224–1231
202. Monico L, Janssens K, Miliani C, Brunetti BG, Vagnini M, Vanmeert F, Falkenberg G, Abakumov A, Lu Y, Tian H, Verbeeck J, Radepon M, Cotte M, Hendriks E, Geldof M, van der Loeff L, Salvant J, Menu M (2013) Degradation process of lead chromate in paintings by Vincent van Gogh studied by means of spectromicroscopic methods. 3. Synthesis, characterization, and detection of different crystal forms of the chrome yellow pigment. *Anal Chem* 85:851–859
203. Monico L, Janssens K, Miliani C, Van der Snickt G, Brunetti BG, Guidi MC, Radepon M, Cotte M (2013) Degradation process of lead chromate in paintings by Vincent van Gogh studied by means of spectromicroscopic methods. 4. Artificial aging of model samples of co-precipitates of lead chromate and lead sulfate. *Anal Chem* 85:860–867
204. Monico L, Janssens K, Vanmeert F, Cotte M, Brunetti BG, Van der Snickt G, Leeuwestein M, Plisson JS, Menu M, Miliani C (2014) Degradation process of lead chromate in paintings by Vincent van Gogh studied by means of spectromicroscopic methods. Part 5. Effects of nonoriginal



- surface coatings into the nature and distribution of chromium and sulfur species in chrome yellow paints. *Anal Chem* 86:10804–10811
205. Monico L, Janssens K, Cotte M, Romani A, Sorace L, Grazia C, Brunetti BG, Miliani C (2015) Synchrotron-based X-ray spectromicroscopy and electron paramagnetic resonance spectroscopy to investigate the redox properties of lead chromate pigments under the effect of visible light (vol 30, pg 1500. *J Anal At Spectrom* 30(2015):2024
 206. Monico L, Janssens K, Cotte M, Sorace L, Vanmeert F, Brunetti BG, Miliani C (2016) Chromium speciation methods and infrared spectroscopy for studying the chemical reactivity of lead chromate-based pigments in oil medium. *Microchem J* 124:272–282
 207. Tan H, Tian H, Verbeeck J, Monico L, Janssens K, Van Tendeloo G (2013) Nanoscale investigation of the degradation mechanism of a historical chrome yellow paint by quantitative EELS mapping of Cr species. *Angew Chem Int Ed* 52
 208. Monico L, Janssens K, Hendriks E, Brunetti BG, Miliani C (2014) Raman study of different crystalline forms of PbCrO_4 and $\text{PbCr}_{1-x}\text{SxO}_4$ solid solutions for the noninvasive identification of chrome yellows in paintings: a focus on works by Vincent van Gogh. *J Raman Spectrosc* 45:1034–1045
 209. Monico L, Janssens K, Alfeld M, Cotte M, Vanmeert F, Ryan CG, Falkenberg G, Howard DL, Brunetti BG, Miliani C (2015) Full spectral XANES imaging using the Maia detector array as a new tool for the study of the alteration process of chrome yellow pigments in paintings by Vincent van Gogh. *J Anal At Spectrom* 30:613–626
 210. Otero V, Pinto JV, Carlyle L, Vilarigues M, Cotte M, Melo MJ (2016) Nineteenth century chrome yellow and chrome deep from Windsor & Newton. *Stud Conserv* 61:1–27
 211. Amat A, Miliani C, Fantacci S (2016) Structural and electronic properties of the PbCrO_4 chrome yellow pigment and of its light sensitive sulfate-substituted compounds. *RSC Adv* 44
 212. Munoz-Garcia AB, Massaro A, Pavone M (2016) Ab Initio Study of $\text{PbCr}(1-x)\text{SxO}_4$ Solid Solution: an Inside Look at Van Gogh Yellow Degradation. *Chem Sci*
 213. Casadio F, Xie S, Rukes SC, Myers B, Gray KA, Warta R, Fiedler I (2011) Electron energy loss spectroscopy elucidates the elusive darkening of zinc potassium chromate in Georges Seurat's *A Sunday on La Grande Jatte-1884*. *Anal Bioanal Chem* 399:2909–2920
 214. Zanella L, Casadio F, Gray KA, Warta R, Ma Q, Gaillard J-F (2011) The darkening of zinc yellow: XANES speciation of chromium in artist's paints after light and chemical exposures. *J Anal At Spectrom* 26:1090–1097
 215. Rosi F, Grazia C, Gabrieli F, Romani A, Paolantoni M, Vivani R, Brunetti BG, Colomban P, Miliani C (2016) UV–Vis–NIR and micro Raman spectroscopies for the non destructive identification of $\text{Cd}_{1-x}\text{ZnxS}$ solid solutions in cadmium yellow pigments. *Microchem J* 124:856–867
 216. Grazia C, Rosi F, Gabrieli F, Romani A, Paolantoni M, Vivani R, Brunetti BG, Colomban P, Miliani C (2016) UV–Vis–NIR and microRaman spectroscopies for investigating the composition of ternary $\text{CdS}_{1-x}\text{Sex}$ solid solutions employed as artists' pigments. *Microchem J* 125:279–289
 217. Van der Snickt G, Dik J, Cotte M, Janssens K, Jaroszewicz J, De Nolf W, Groenewegen J, Van der Loeff L (2009) Characterization of a degraded cadmium yellow (CdS) pigment in an oil painting by means of synchrotron radiation based X-ray techniques. *Anal Chem* 81:2600–2610
 218. Van der Snickt G, Janssens K, Dik J, De Nolf W, Vanmeert F, Jaroszewicz J, Cotte M, Falkenberg G, Van der Loeff L (2012) Combined use of synchrotron radiation based micro-X-ray fluorescence, Micro-X-ray Diffraction, Micro-X-ray absorption near-edge, and micro-fourier transform infrared spectroscopies for revealing an alternative degradation pathway of the pigment cadmium yellow in a painting by Van Gogh. *Anal Chem* 84:10221–10228
 219. Mass J, Sedlmair J, Patterson CS, Carson D, Buckley B, Hirschmugl C (2013) SR-FTIR imaging of the altered cadmium sulfide yellow paints in Henri Matisse's *Le Bonheur de vivre* (1905–6)—examination of visually distinct degradation regions. *Analyst* 138:6032–6043
 220. Mass JL, Opila R, Buckley B, Cotte M, Church J, Mehta A (2013) The photodegradation of cadmium yellow paints in Henri Matisse's *Le Bonheur de vivre* (1905–1906). *Appl Phys A Mater Sci Process* 111:59–68
 221. Uffelman ES, Hobbs PA, Barisas DAG, Mass JL (2013) pXRF analyses of Louise Herreshoff's paintings in relation to CdS and other pigment degradation issues. *Appl Phys A Mater Sci Process* 111:9–14
 222. Pouyet E, Cotte M, Fayard B, Salome M, Meirer F, Mehta A, Uffelman ES, Hull A, Vanmeert F, Kieffer J, Burghammer M, Janssens K, Sette F, Mass J (2015) 2D X-ray and FTIR micro-analysis of the degradation of cadmium yellow pigment in paintings of Henri Matisse. *Appl Phys A Mater Sci Process* 121:967–980



- 2124 223. Voras ZE, deGhetaldi K, Wiggins MB, Buckley B, Baade B, Mass JL, Beebe TP Jr (2015) ToF-
2125 SIMS imaging of molecular-level alteration mechanisms in Le Bonheur de vivre by Henri Matisse.
2126 Appl Phys A Mater Sci Process 121:1015–1030
- 2127 224. Ayalew E, Janssens K, De Wael K (2016) Unraveling the reactivity of minium toward bicarbonate
2128 and the role of lead oxides therein. Anal Chem 88:1564–1569
- 2129 225. Vila A, Monrad K, Wadum J, Filtenborg T (2014) As time passed by came sunset. Christen Købke's
2130 'View of Lake Sortedam', its genesis and colour changes. In: Sgamellotti A, Brunetti BG, Miliani C
2131 (eds) Science and art. The painted surface. Royal Society of Chemistry, London, pp 354–372
- 2132 226. Samain L, Silversmit G, Sanyova J, Vekemans B, Salomon H, Gilbert B, Grandjean F, Long GJ,
2133 Hermann RP, Vincze L, Strivay D (2011) Fading of modern Prussian blue pigments in linseed oil
2134 medium. J Anal At Spectrom 26:930–941
- 2135 227. Samain L, Gilbert B, Grandjean F, Long GJ, Strivay D (2013) Redox reactions in Prussian blue
2136 containing paint layers as a result of light exposure. J Anal At Spectrom 28:524–535
- 2137 228. Samain L, Grandjean F, Long GJ, Martinetto P, Bordet P, Strivay D (2013) Relationship between
2138 the synthesis of prussian blue pigments, their color, physical properties, and their behavior in paint
2139 layers. J Phys Chem C 117:9693–9712
- 2140 229. Samain L, Grandjean F, Long GJ, Martinetto P, Bordet P, Sanyova J, Strivay D (2013) Synthesis
2141 and fading of eighteenth-century Prussian blue pigments: a combined study by spectroscopic and
2142 diffractive techniques using laboratory and synchrotron radiation sources. J Synchrotron Radiat
2143 20:460–473
- 2144 230. Gervais C, Languille M-A, Reguer S, Gillet M, Pelletier S, Garnier C, Vicenzi EP, Bertrand L
2145 (2013) Why does Prussian blue fade? Understanding the role(s) of the substrate. J Anal At Spectrom
2146 28:1600–1609
- 2147 231. Cotter MJ, Meyers P, Vanzelst L, Sayre EV (1973) Authentication of paintings by Blakelock, RA
2148 through neutron-activation autoradiography. J Radioanal Chem 15:265–285
- 2149 232. Alfeld M, Laurenze-Landsberg C, Denker A, Janssens K, Noble P (2015) Neutron activation
2150 autoradiography and scanning macro-XRF of Rembrandt van Rijn's Susanna and the Elders
2151 (Gemaldegalerie Berlin): a comparison of two methods for imaging of historical paintings with
2152 elemental contrast. Appl Phys A Mater Sci Process 119:795–805
- 2153 233. Seim C, Laurenze-Landsberg C, Schroeder-Smeibidl B, Mantouvalou I, de Boer C, Kanngiesser B
2154 (2014) Old traces, read anew—'The Reading Hermit' painting in the light of X-ray fluorescence.
2155 J Anal At Spectrom 29:1354–1360
- 2156 234. Van der Snickt G, Legrand S, Caen J, Vanmeert F, Alfeld M, Janssens K (2016) Chemical imaging
2157 of stained-glass windows by means of macro X-ray fluorescence (MA-XRF) scanning. Microchem J
2158 124:615–622
- 2159 235. Ricciardi P, Legrand S, Bertolotti G, Janssens K (2016) Macro X-ray fluorescence (MA-XRF) scanning
2160 of illuminated manuscript fragments: potentialities and challenges. Microchem J 124:785–791
- 2161 236. Targowski P, Pronobis-Gajdzis M, Surmak A, Iwanicka M, Kaszewska EA, Sylwestrzak M (2015)
2162 The application of macro-X-ray fluorescence and optical coherence tomography for examination of
2163 parchment manuscripts. Stud Conserv 60:S167–S177
- 2164 237. Jackall Y, Delaney JK, Swicklik M (2015) 'Portrait of a woman with a book': a 'newly discovered
2165 fantasy figure' by Fragonard at the National Gallery of Art, Washington. Burlingt Mag 157:248–254
- 2166 238. Bacci M, Picollo M (1996) Non-destructive spectroscopic detection of cobalt(II) in paintings and
2167 glass. Stud Conserv 41:136–144
- 2168 239. Bacci M, Picollo M, Trumpy G, Tsukada M, Kunzelman D (2007) Non-invasive identification of
2169 white pigments on 20th-century oil paintings by using fiber optic reflectance spectroscopy. J Am
2170 Inst Conserv 46:27–37
- 2171 240. Delaney JK, Zeibel JG, Thoury M, Littleton R, Palmer M, Morales KM, de la Rie ER, Hoenigswald
2172 A (2010) Visible and infrared imaging spectroscopy of picasso's harlequin musician: mapping and
2173 identification of artist materials in situ. Appl Spectrosc 64:584–594
- 2174 241. Gautier G, Bezur A, Muir K, Casadio F, Fiedler I (2009) Chemical fingerprinting of ready-mixed
2175 house paints of relevance to artistic production in the first half of the twentieth century. Part I:
2176 Inorganic and organic pigments. Appl Spectrosc 63:597–603
- 2177 242. Green AA, Berman M, Switzer P, Craig MD (1988) A transformation for ordering multispectral
2178 data in terms of image quality with implications for noise removal. IEEE Trans Geosci Remote Sens
2179 26:65–74
- 2180 243. Nielsen AA (2011) Kernel maximum autocorrelation factor and minimum noise fraction transfor-
2181 mations. IEEE Trans Image Process 20:612–624
- 2182

